



SCHOOL OF ENGINEERING
UNIVERSITY CARLOS III OF MADRID

Trajectory Analysis of a Cubesat Lunar Mission

A thesis submitted for the degree of
Master in Aeronautical Engineering

Author: Nereida Agüera López
Supervisor: Manuel Sanjurjo Rivo

Leganés
June 10, 2017

Contents

Abstract	VII
Resumen	IX
1 Introduction	1
2 Motivation	5
2.1 SmallSats and Cubesats	5
2.2 Micropulsion	7
2.3 Lunar exploration	9
3 State of the art	13
3.1 Impulsive burn orbit transfers	13
3.2 Limited burn orbit transfers	15
4 Background	19
4.1 Dynamic models	19
4.1.1 Planar Circular Restricted Three-Body Problem	19
4.1.2 Planar Bicircular Restricted Four-Body Problem	24
4.1.3 Transforming coordinates between rotating frames	26
4.2 Invariant manifolds theory	27
5 Initial Guess Construction	31
5.1 Initial Guess based on the invariant manifolds of the Lagrange points	31
5.1.1 Manifolds construction	32
5.1.2 Earth escape leg	37

5.1.3	Moon capture leg	38
5.1.4	Trajectory patching	40
5.2	Initial guess based on the classical two-impulse trajectories	42
5.2.1	Problem definition	42
5.2.2	Genetic algorithm optimization	42
6	Optimization Problem	49
6.1	Optimal Control	49
6.2	Problem definition	52
7	Results and Discussion	55
7.1	Optimization results	55
7.1.1	Trajectory A	56
7.1.2	Trajectory B	58
7.1.3	Trajectory C	60
7.1.4	Trajectory D	62
7.2	Trajectory comparison and possible lunar missions	64
8	Project Management	67
8.1	Time Management	67
8.2	Cost Management	68
9	Conclusions and Future Work	71
Bibliography		77

List of Figures

2.1.1	Graphical description of the Cubesat or <i>U-Spacecraft</i> concept	6
3.1.1	Different approaches to Earth-Moon transfers [28].	14
3.2.1	Lunar trajectories in the Earth-Moon rotating frame. Distance unit is the Earth radius, R_E [35].	16
3.2.2	Earth-Moon transfer trajectory phases [41].	16
4.1.1	General configuration for the CR3BP [48].	20
4.1.2	Inertial and rotating frames in the CR3BP. The rotating coordinate system with coordinates x and y moves counterclockwise with unit angular velocity relative to the inertial frame with coordinates X and Y [28].	21
4.1.3	Zero-velocity contours of the Earth-Moon system.	22
4.1.4	Realms of possible motion for five different energy levels. The shaded gray areas corresponds to the forbidden realm.	23
4.1.5	Lagrange points for the Earth-Moon PCR3BP.	24
4.1.6	Rotating coordinate system. The positions of the Earth (E), Moon (M) and Sun (S) are depicted. The short-dashed circles represent the Earth's and Moon's orbits in the non- rotating coordinate system, and long-dashed circle represents the Sun's orbit in the rotating coordinate system [49].	26
4.2.1	Stable and unstable manifolds of a periodic orbit whose monodromy matrix has one eigenvalue inside and one outside the unit circle [51].	29
5.1.1	Sketch of the desired initial guesses to be obtained based on the dynamics of the invariant manifolds [28]. (—) Earth-Moon leg, (—) Sun-Earth leg.	32
5.1.2	Location of the libration points. (—) Collinear libration points, (—) Equilateral libration points, m_E , m_M and m_S refer to the Earth, Moon and Sun masses, respectively.	33
5.1.3	Examples of L_2 periodic orbits of different amplitude.	35

5.1.4 A simple way to compute an approximation of the two branches of the unstable ($W^{U\pm}$) or stable ($W^{S\pm}$) manifolds of a periodic orbit [28].	36
5.1.5 (—) Stable manifolds, (—) Unstable manifolds	37
5.1.6 Manifold and phase space at S_A for $\varphi_A = 90^\circ$	37
5.1.7 Manifold and phase state at S_B for $\varphi_B = 90^\circ$	38
5.1.8 Manifold trajectories and phase space at Section B for $\varphi_0 = 210^\circ$	39
5.1.9 Manifold trajectories and phase space at Section B for $\varphi_0 = 225^\circ$	39
5.1.10 Examples of complete initial guess trajectories. $m_{M,F}$ and $m_{M,P}$ refer to the Moon mass position at the end of the trajectory and at the patching instant between the Earth escape and Moon capture legs; the Moon's orbit corresponds to the dashed line (—); m_E refers to the Earth mass; L_2 refers to the Sun-Earth L_2 libration point.	41
5.1.11 Complete trajectory starting from a GEO orbit, selected Initial Guess for trajectory optimization.	41
5.2.1 Direct shooting of initial guess solutions [30].	43
5.2.2 Sketch of the genetic algorithm process.	45
5.2.3 Example of the genetic algorithm operators.	45
5.2.4 Pareto front obtained from the genetic algorithm implementation in terms of the two specified objective functions, (•) Selected initial guess.	46
5.2.5 Population of chromosomes in terms of one of the objective functions, J_1 , and the time of transfer, δ . (•) Selected initial guess.	46
5.2.6 Population of chromosomes in terms of one of the objective functions, J_2 , and the time of transfer, δ . (•) Selected initial guess.	47
5.2.7 Selected initial guess for the Earth-Moon transfer.	47
6.1.1 Hermite-Simpson collocation method (third-degree interpolant) [62].	51
7.1.1 Trajectory A results.	57
7.1.2 Trajectory B results.	60
7.1.3 Trajectory C results.	62
7.1.4 Trajectory D results.	64

List of Tables

2.2.1 Micropropulsion devices performance data [6,7,9,10,11,12,13,14,15].	8
5.1.1 Characteristic magnitudes for the PCR3BP Sun-Earth and Earth-Moon systems.	33
7.2.1 Details of optimized trajectories.	64
8.1.1 Gantt chart	68
8.2.1 Labor cost details.	69
8.2.2 Equipment cost details.	69
8.2.3 Software cost details.	69
8.2.4 Total project costs.	69

Abstract

In the last decades, we have witnessed a renewed interest of the space community in the Moon. From a scientific standpoint, future lunar missions could help us understand the formation of the Solar System and the Earth, among others. Moreover, unmanned lunar exploration not only constitutes an end in itself, but it is also a key enabler for the long term goal of undertaking future human missions to explore the Moon and then, Mars. In this regard, Cubesats represent a unique low-cost yet efficient way for technology demonstration and scientific research that can help shorten the time and resources needed to achieve those long-term goals. Indeed, the flourishing of SmallSats, together with the advancement of miniaturized technology and electric micropulsion, among others, have triggered a paradigm shift in the space community towards a low-cost access to space. In this context, many ambitious Cubesat lunar missions have already been proposed, most studies focusing on the system level analysis. However, Cubesat Moon missions also represent a challenge from the trajectory design point of view, due to the sizing and propulsive limitations they entail. The goal of this work is to provide a detailed procedure to design Earth-Moon Cubesat transfer trajectories. For that, two different approaches well-known in the literature for traditional (impulsive) transfers have been used to generate initial guess trajectories, one of them exploiting the dynamics of the invariant manifolds of the libration points in the three-body problem, the other using a four body dynamic model and genetic optimization. These initial guesses were then adapted and optimized using Non-Linear Programming methods to obtain minimum-fuel Earth-Moon transfers coherent with the Cubesat constraints in the four-body dynamics framework. As a result, promising transfer trajectories starting from Geosynchronous Earth Orbit were obtained, demonstrating the feasibility of this kind of Cubesat transfers from the Astrodynamics point of view. Besides, the potential of the procedures detailed lies mainly on their versatility and the possibility of easily tuning them for the particular needs of a mission, serving then as a powerful mission analysis tool.

Resumen

En las últimas décadas, hemos sido testigos del resurgir de un interés renovado en la Luna por parte del sector espacial. Desde el punto de vista científico, la exploración lunar podría ayudarnos a entender la formación del Sistema Solar y de la Tierra, entre otros. Además, las misiones lunares no tripuladas no sólo constituyen un fin en sí mismo, sino que son fundamentales y necesarias para hacer posible el objetivo a largo plazo de enviar misiones tripuladas para explorar la Luna y también Marte. En este aspecto, los *Cubesats* representan una alternativa única de bajo coste y muy eficiente para realizar demostraciones tecnológicas e investigación científica que puede acortar el tiempo y los recursos necesarios para lograr estos objetivos a largo plazo. De hecho, el auge de los *SmallSats*, la miniaturización de la tecnología y la micropropulsión eléctrica, entre otros, han impulsado un cambio de paradigma en el ámbito espacial hacia un acceso al espacio de bajo coste. En este contexto, muchas misiones lunares muy ambiciosas usando Cubesats ya han sido propuestas, sin embargo, la mayoría de estos estudios se centran en el análisis de misión a nivel de sistema. No obstante, estas misiones también representan un desafío desde el punto de vista del diseño de trayectorias, debido a las limitaciones propulsivas y de tamaño que llevan. El objetivo de este trabajo es ofrecer un método detallado para diseñar trayectorias de transferencia Tierra-Luna con Cubesats. Para ello, dos enfoques extraídos de la literatura diseñados para transferencias tradicionales (impulsivas) se han empleado para generar estimaciones iniciales, uno de ellos basado en la dinámica de los puntos de Lagrange del problema de los tres cuerpos, mientras que el otro utiliza un algoritmo de optimización genética en el contexto del problema de los cuatro cuerpos. Estas estimaciones iniciales fueron más tarde adaptadas y optimizadas usando métodos de Programación No Lineal para obtener transferencias Tierra-Luna con el mínimo gasto de combustible y consistentes con las limitaciones de un Cubesat. Como resultado, se han obtenido prometedoras trayectorias de transferencia partiendo desde órbitas geosíncronas, demostrando la viabilidad de este tipo de misiones con Cubesats desde el punto de vista astrodinámico. Además, el potencial de los métodos detallados yace fundamentalmente en su versatilidad y la capacidad de adaptarlos fácilmente a los requisitos de cada misión, constituyendo una herramienta muy útil para el análisis de misión.

Nomenclature

<i>ANN</i>	A rtificial N eural N etwork
<i>CLE</i>	C ubesat L ow frequency E xplorer
<i>CR3BP</i>	C ircular R estricted T hree B ody P roblem
<i>EA</i>	E volutionary A lgorithm
<i>ENC</i>	E volutionary N euro C ontrol
<i>FEEP</i>	F ield EE lectric P ropulsion
<i>GEO</i>	G eosynchronous E arth O rbit
<i>GPM</i>	G auss P seudospectral M ethod
<i>GPOPS</i>	G auss P seudospectral O ptimization S oftware
<i>GPS</i>	G lobal P ositioning S ystem
<i>GRAIL</i>	G ravity R ecoveries and I nterior L aboratory
<i>GS2BI</i>	G eometrically S imilar to the 2 - B urn I mpulsive
<i>GS3BI</i>	G eometrically S imilar to the 3 - B urn I mpulsive
<i>iEPS</i>	I on E lectrospray P ropulsion S ystem
<i>IPOPT</i>	I nterior P oint O PTimizer
<i>LADEE</i>	L unar A tmosphere and D ust E nvironment E xplorer
<i>LEAG</i>	L unar E xploration A nalysis G roup
<i>LEO</i>	L ow E arth O rbit
<i>LLO</i>	L ow L unar O rbit
<i>LRO</i>	L unar R ecognnaissance O rbit
<i>MiXI</i>	M iniature X enon I on
<i>MPACS</i>	M icro P ropulsion A ttitude C ontrol S ystem
<i>NCLE</i>	N etherlands- C hina L ongwavelength E xplorer
<i>NLP</i>	N on- L inear P rogramming

<i>NSGA</i>	Non-dominated Sorting Genetic Algorithm
<i>OLFAR</i>	Orbiting Low Frequency ARray
<i>PBRFBP</i>	Planar Bicircular Restricted Four Body Problem
<i>PCR3BP</i>	Planar Circular Restricted Three Body Problem
<i>PPT</i>	Pulsed Plasma Thruster
<i>PSDS3</i>	Planetary Science Deep Space SmallSat Studies
<i>SKG</i>	Strategic Knowledge Gaps
<i>SMART</i>	Small Missions for Advanced Research in Technology
<i>SOI</i>	Sphere Of Influence

Chapter 1

Introduction

The Moon has been the object of study of countless works for centuries, starting with Galileo's telescopic observations as early as 1609. Even though the interest on the Moon seemed to peak during the years of the *space race*, it is very clear that lunar exploration can still foster human knowledge in many areas, for instance, it could be the key to understand the formation of the Solar System, the Earth and its biosphere. Moreover, even though many scientific objectives could be achieved robotically, it is well known that space science could benefit from future human lunar missions. This fact reinforces the urge for unmanned exploration missions in order to understand the lunar resource potential, the lunar environment and its effect on human life, and how to work and live on the lunar surface, among others.

In this regard, although lunar exploration is guaranteed to offer significant scientific and technological return, the high costs and elevated risks involved in sending conventional spacecraft to the Moon have significantly restricted the number of such missions.

However, we have recently witnessed a renewed interest of the space community on the Moon with several successful missions being launched in the last two decades and many others underway. This new trend is greatly related to a somewhat greater change in the space industry which it is generally referred to as the *New Space* paradigm. The emergence of SmallSats and the increasing presence of electric space propulsion are some of the key drivers of this paradigm shift.

SmallSats offer a uniquely inexpensive pathway to undertake ambitious lunar missions. In particular, CubeSats, which are nanosatellites built in a modular way using 10 cm cubic units, are particularly attractive due to their low development and mission costs, ease of construction, frequent launch opportunities (they can be launched as secondary payload or using dedicated launchers) and high degree of mission flexibility. Besides, Cubesats have effectively reduced the cost to participate in space activities, therefore triggering numerous developments across industry, government and academic environments.

Concerning lunar exploration, multiple Cubesat Moon missions have been proposed in recent years, most studies focusing on the system-level analysis. However, the usage of Cubesats also represents a challenge from the Astrodynamics point of view, due to the

sizing and propulsive limitations. In this regard, a framework for trajectory design for Earth-Moon Cubesat transfers has not been provided yet.

Talking about trajectory design, classical Earth-Moon transfers relied in the *patched conics approach*; however, the high ΔV needed at arrival in order to overcome the hyperbolic excess velocity highly limited the mission design possibilities. Low energy transfers, which exploit the *N-body dynamics*, appeared as a solution, making possible missions which classical approaches could not. Besides, further studies showed that the cost of low energy transfers could be further reduced by using low-thrust propulsion, exploiting both the simultaneous gravitational attractions of the Sun, the Earth and the Moon, and the high specific impulse provided by the low-thrust electric engines. Indeed, the electric propulsion systems have also received an increasing attention in the last decades. The ESA mission SMART-1, launched in 2003, showed how to fly to the Moon electrically, opening the path to more unconventional approaches to trajectory design.

The motivation behind the work presented in this report emerges naturally from acknowledging this space paradigm shift and the need to develop a dedicated trajectory design framework that can fit this newly envisioned lunar mission concepts and allow the exploitation of Cubesats, miniaturized technology, micropropulsion,...to enable *low-cost* access to space.

In this way, the goal of this work is to provide a procedure for designing feasible Cubesats Earth-Moon trajectories. For that, two different approaches well-known in the literature for traditional (impulsive) transfers have been used to generate initial guess trajectories that were then adapted to the Cubesat microthrust scenario using Non-Linear Programming optimization methods in the four-body dynamics framework.

On one hand, initial guess transfer trajectories have been designed by dividing the Sun-Earth-Moon-Spacecraft four body problem into two three-body problems and exploiting the dynamics of the invariant manifolds of the Lagrange points. On the other hand, an alternative procedure to generate initial guess trajectories using a more holistic approach to the four-body problem together with genetic optimization is also presented.

As a final step, the initial guess trajectories were optimized to obtain minimum-fuel Earth-Moon transfers coherent with the Cubesat sizing and propulsive constraints. Although the results presented here do not intend to be an exhaustive description of possible Earth-Moon transfer trajectories, very promising trajectories were obtained, serving as a proof of concept that these kind of Cubesat transfers are feasible from an Astrodynamics point of view. More importantly, two different procedures for trajectory generation are detailed and could be easily used as mission analysis tools for a wide variety of SmallSat Moon missions.

The project contents have been distributed into nine chapters, that are presented below:

- Chapter 1 corresponds to this *Introduction*, in which a brief outline of the project is given, together with a concise description of the goals, motivation and throughput of the work.
- Chapter 2, *Motivation*, provides the technical but also social and economic context, offering a rationale and helping understand the relevance of the work presented.

- Chapter 3 contains a thorough *State of the art* revision, consisting on a summarized review of the Earth-Moon trajectory design contributions found in the literature.
- Chapter 4, *Background*, provides an explanation of some dynamical and mathematical concepts whose understanding is key for the comprehension of the trajectory design procedures presented in this work.
- Chapter 5 deals with the *Initial Guess Construction*, namely, two different trajectory design methods extracted from the impulsive transfers literature are implemented in order to find initial solutions for the Cubesat Earth-Moon transfers.
- Chapter 6 provides a detailed explanation of the *Optimization problem*, providing some background on the Optimal Control methods used in this work as well as a detail description of the problem at hand.
- Chapter 7 gathers the *Results and discussion*, in other words, several optimized trajectories obtained with the procedures explained in this work are presented and analyzed.
- Chapter 8 deals with the *Project Management* aspect of the project, namely, time and cost management analysis.
- Chapter 9 includes some final *Conclusions and Future Work* to summarize the main points included in this work together with an awareness about its limitations and ideas on how to overcome them, as well as indications on related and interesting further research.

Chapter 2

Motivation

An understanding of the current technological and socioeconomic context of the space industry is key in order to grasp the rationale behind this work. That is why the goal of this chapter is to give some insight into the main ideas enabling and giving purpose to Earth-Moon Cubesat missions. Three topics will be discussed: SmallSats and Cubesats, miniaturized technology -particularly, micropulsion-, and lunar exploration. In this way, we will understand how Cubesats and miniaturized technology have shaped the new trends in the space industry, what are the advantages of using Cubesats versus conventional satellites, and finally, why it is relevant to send Cubesats to the Moon.

2.1 SmallSats and Cubesats

The term *SmallSat* applies to those spacecraft whose weight is lower than 180 kg [1]. Besides, they can be further clasified into the following categories:

- Minisatellite, 100-180 kilograms
- Microsatellite, 10-100 kilograms
- Nanosatellite, 1-10 kilograms
- Picosatellite, 0.01-1 kilograms
- Femtosatellite, 0.001-0.01 kilograms

Although once conceived as mere experimental prototypes, and later relegated to LEO missions, SmallSats play now a prominent role in the space industry. Indeed, their potential to perform scientific space missions at a much lower cost than their large spacecraft counterparts has become evident. For instance, as of March 2017, NASA has selected ten studies as part of the Planetary Science Deep Space SmallSat Studies (PSDS3) program to develop deep space science investigation mission concepts with SmallSats that will study Venus, Mars, asteroids, etc [2].

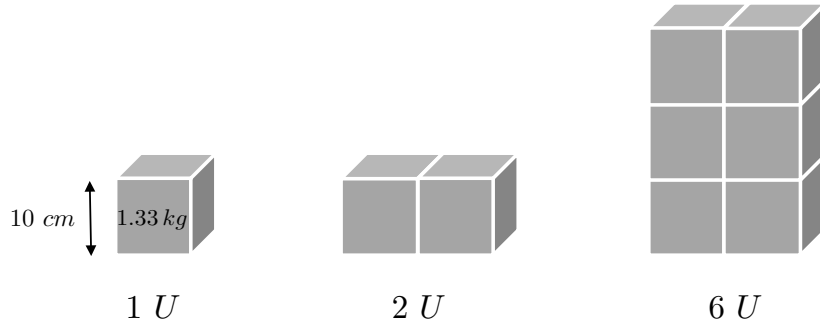


Figure 2.1.1: Graphical description of the Cubesat or *U-Spacecraft* concept

On the other hand, the so called *Cubesats* represent a subset of nanosatellites whose size and weight is standardized. The *Cubesat standard* was coined in 1999 by Jordi Puig-Suari of California Polytechnic Institute (Cal Poly) and Robert Twiggs of Stanford University, and its basic unit (1 U) consists on a 10-cm cube with mass of no more than 1 kg [3], which was later updated to 1.33 kg [4]. At present, the term *Cubesat* refers not only to 1 U *spacecraft*, but also to larger spacecraft which are still built using this same standard -even up to 12 U-in a modular way, as depicted in Figure 2.1.1.

The origin of Cubesats is eminently academical. They were conceived as a way to promote the students' participation in satellite development: traditional spacecraft design, on the contrary, required times in the multi-year range and was too capital and expertise intensive [3].

Nowadays, Cubesats offer a unique opportunity for scientific research and technology development in the space environment. The exponential growth of their potential applications represents a disruption in the current space industry since they could replace large conventional satellites in many cases, creating a real *paradigm shift*. This is the reason why they are no longer attractive just for small budget ventures but also medium and large aerospace companies are investing in Cubesat missions.

Besides, thanks to the low-cost associated with the development of small satellites, together with the possibility of being launched as *secondary payload*, they have fostered space initiatives in emerging countries where little resources have been traditionally allocated to space science and technology. In this way, Cubesats have the potential to make a deep social impact as well since they could be a way to help increase the long-term intellectual capital of those countries. For instance, Argentina launched the 6-kg educational satellite *Pehuensat-I* in 2007, that enabled students to broadcast messages in several languages. Some other examples are Brazil launching the *NanoSatC-Br1* in 2014 to provide monitoring of Earth's magnetosphere, or the Turkish *ITUpSAT 1*, launched in 2009 with an educational and technological development purpose [3].

At this stage, Cubesats are normally launched as secondary payload, which offers two main advantages: on one hand, this lowers significantly the price per kg launched, and on the other hand, it increases the launch opportunities for a given budget. In this sense, the *Cubesat Specification* has helped to reduce the cost of launch and deployment of small satellites [4,5]. However, the dependence on regular launchers also limits the use of small

satellites to their fullest potential, for instance, due to orbit limitations, since they have to adapt to the primary satellite mission; or due to design constraints, in order to make sure that the *piggy-back* does not present a hazard for the primary payload. It is due to these reasons, among others, that we are witnessing a growing focus on the development of exclusive vehicles for the launch of small satellites.

2.2 Micropulsion

The rapid Cubesat development has been done in parallel and thanks to an equally rapid development of nano-, micro- and mini- technologies that have led to sensors, instruments, materials,... compatible with the sizing constraints of the Cubesats. These systems, when incorporated on the Cubesat frame, enable it to perform the desired experiment or activity. Although Cubesat missions are normally single-purpose and simpler than traditional ones, their lower cost and easier accessibility allow them to provide a large scientific and/or technological return.

This work will deal with an Earth-Moon Cubesat trajectory design from an Astrodynamics standpoint, so we will not include here a thorough discussion on the Cubesats from the system level perspective. However, some knowledge on the state of the art performances of Cubesat-compatible propulsion subsystems is of particular importance, since this will serve as an input for the trajectory control optimization and will somehow determine the transfer possibilities.

Propulsion systems are required to continue the rapid growth and increased mission capability of CubeSats. Nonetheless, due to limitations in the CubeSat platform itself, advancement of these systems from concept to flight heritage is slow [6]. In this attempt, two approaches have been observed, in general. One option has been to try to miniaturize systems that are well-known and are operating in traditional large-scale spacecraft. The other option is to rely on novel physical and chemical mechanisms and explore new technologies to develop micropulsion systems [7].

Concerning the type of propulsion and following the conventional space propulsion classification, we have two main choices based on their primary mechanism of thrust generation: chemical and electrical micropulsion. Besides, some propellant-less solutions have emerged, like solar sails and electrodynamic tethers.

In the chemical propulsion field, efforts have been made to try to miniaturize traditional space propulsion systems; however, issues such as the leakage or toxicity of propellants, together with the rapid decrease of thrust and specific impulse have complicated the development of these systems. Research on micronozzles, new propellants and higher performance valves is still ongoing. Besides, the combustion process creates complications when trying to launch a CubeSat as a secondary payload due to limits on pyrotechnics and stored chemical energy. An exception to this are cold gas propulsion systems, in which the gas is accelerated without any combustion or heat addition. Because of its low power operation and simplicity, cold gas systems have flight heritage on CubeSats; however, they offer significantly lower Isp and deliver less ΔV for the same spacecraft because the energy

stored within chemical bonds is not utilized [6].

Electric micropropulsion is right now an active field of research. In general, there are three types of electric propulsion systems: electrothermal, electromagnetic, and electrostatic. In general, these systems generate less thrust than cold gas and chemical propulsion systems; however, the higher specific impulse makes them really appealing for Cubesat interplanetary missions. In this case, miniaturization is also challenging. For instance, a large powerful magnetic field needs to be applied to the miniaturized ion thruster to allow ion production in chambers, which may be smaller than the mean free path of the ionizing electrons. As an alternative to miniaturization of existing concepts, there is a wide range of newly envisioned electric micropropulsion technologies under development: colloid thrusters, laser ablation thrusters, field emission electric propulsion, vacuum arc thrusters, etc [7].

In this work, due to both the strictly limited volume and mass of Cubesats and the interplanetary character of the mission proposed, we will particularly focus on the potential offered by high specific impulse electric micropropulsion systems, which will allow to greatly cut down on propellant mass [8]. Table 2.2.1 categorizes some examples of these promising technologies and their declared performances, although it does not intend to be an exhaustive list of the existing electrical micropropulsion devices. Please refer to [6,7] for a more detailed taxonomy of Cubesat compatible propulsion systems. Besides, it is important to bear in mind that there is a large variation in technology readiness levels (TRLs), which makes a system-level comparison really challenging. On top of that, sometimes information about specifications is limited or not available in publicly released literature.

Name	Manufacturer	Thrust [μN]	Specific Impulse [s]	Power [W]	Technology
RIT- μX	Astrium	40 - 718	500 - 3500	10 - 70	Miniaturized Ion Thruster
μNRIT	Astrium	200 - 500	1236 - 2609	30	Miniaturized Ion Thruster
MiDGIT	QinetiQ	200 - 480	400 - 1100	22 - 29	Miniaturized Ion Thruster
MiXI	JPL	10-1500	2500-3200	13-50	Miniaturized Ion Thruster
BIT-3	Busek	600-1100	1200-2000	55-75	Miniaturized Ion Thruster
SPT-20M	KhAI	4000	1400	<100	Miniaturized Hall thruster
MPACS μPPT	Busek	<400	827	<10	Miniaturized PPT
Altas FT-150	Alta	0.1 - 150	3000 - 4500	6	FEEP
iEPS	MIT	100	2000	2	Electrospray
BET 100 μN	Busek	5-100	1000-1800	5.5	Electrospray

Table 2.2.1: Micropropulsion devices performance data [6,7,9,10,11,12,13,14,15].

In this work, we will not restrict the analysis to a certain type of micropropulsion technology but instead, representative values of thrust and specific impulse will be taken, coherently with Table 2.2.1, to analyze the feasibility of the Earth-Moon Cubesat transfers and optimize the trajectory design.

2.3 Lunar exploration

Historically speaking, the modern study of the Moon as a planetary body started with Galileo's telescopic observations in 1609 [16]. However, most of the knowledge about the Moon that we have acquired since comes from direct investigation by space probes, mainly during the second half of the last century.

During those years, the *space race* between the Soviet Union and the United States acquired an important focus on lunar exploration that led to the fulfillment of several milestones. For instance, the Soviet Union's *Luna* 2 was the first spacecraft to reach the Moon in 1959 and *Luna* 9 soft-landed and took surface images in 1966. Of course, it is very well-known that this *race* culminated with the landing of the first humans on the Moon in 1969, as part of the United States' *Apollo program*.

In particular, the *Apollo program* provided unprecedented scientific information through remote-sensing observations but also due to lots of surface experiments and sample returns. On the other hand, the Soviet Union's *Lunokhods* rovers made measurements of regolith's mechanical properties and composition, and surface radiation environment, among others.

The new era of lunar exploration started in the 1990s, after an almost 20-year gap, with the Hiten, Clementine and Lunar Prospector spacecraft. These missions helped to renew the interest of the space community on the Moon by evidencing its geological diversity and successfully demonstrating new technologies and concepts, like low energy innovative transfers. As a demonstration of this returning enthusiasm on lunar exploration, just in the last two decades, the following missions have been launched: SMART-1 (2003, ESA), Kaguya (Japan, 2007), Chang'e-1 and Chang'e-2 (2007 and 2010, China), Chandrayaan-1 (2008, India), LRO (2009, NASA), GRAIL (2012, NASA) and LADEE (2013, NASA) [16].

Concerning near-term future lunar exploration, this renewed interest in the Moon does not seem to be fading away, with tentative plans for a number of prospective lunar missions. However, it seems likely that these missions will probably have to adapt to the current changes in the space industry. For instance, private initiatives, such as Google Lunar X-Prize, might be responsible for future lunar exploration missions.

From a scientific standpoint, there are three key areas in which lunar exploration can foster human knowledge [16]:

- The Moon preserves geochemical and geophysical information on the origin and evolution of the Earth-Moon system and in general, on the geological evolution of a rocky planet.
- The lunar surface might allow us to understand the formation of the Solar System, the Earth and its biosphere, since it contains remains of interplanetary dust, meteorite flux and other remnants of inner Solar System processes.
- The Moon has great potential as a platform for astronomical and in general, scientific investigations, such as low-frequency radio astronomy from the far-side.

Although some scientific objectives can be achieved robotically, lunar science and in general, space science could greatly benefit from human missions in the long term. Follow-

ing this line of thought, the Lunar Exploration Analysis Group (LEAG) concluded in the 2016 annual review that there are no Strategic Knowledge Gaps (SKGs) that would prevent the flight of any human mission for a duration of less than 28 days. Nonetheless, several SKGs should be addressed to increase the safety of these potential missions. These SKGs fall under three main groups [17]:

- *Understand the lunar resource potential.* This would enable future missions to use locally sourced resources. For that, a deep understanding of the distribution, abundance and composition of these resources is critical. For instance, the water ice and other volatile chemicals cold trapped in the polar regions are of special interest.
- *Understand the lunar environment and its effects on human life.* This includes the study of radiation, illumination, plasma and dust, and the maintenance of peak human health in this environment.
- *Understand how to work and live on the lunar surface.* This topic deals with life support, mobility, energy production and storage, and resource prospection, among others.

The potential role of small satellites in this context is critical, since they would enable the closure of several SKGs with lower cost and fast development. Besides, the cheap cost outweighs some of the uncertainty, providing a pathway to perform riskier missions.

Following this line of thought, the utility of CubeSats is rapidly increasing with a wide range of Lunar CubeSat missions being proposed and developed for flight. A first-order design guideline for a lunar Cubesat at system-level is given in [18]. In this case, the design is based on a 3 U cubesat propelled by a MiXI thruster (see Table 2.2.1) and the study supports the feasibility of performing lunar Cubesat missions.

Several of the lunar cubesat initiatives that are currently underway focus on the understanding of the lunar resource potential. For example, the Lunar Polar Hydrogen Mapper (*LunaH-Map*) is being developed at Arizona State University in partnership with NASA's Jet Propulsion Laboratory and others, and aims to produce the most detailed map to date of the Moon's water deposits [19]. Alternatively, it is worth mentioning *Lunar Flashlight*, an exciting new mission concept that was recently selected by NASA's Advanced Exploration Systems program and that is planned to be launched on the Space Launch System's Exploration Mission-1 (EM-1) as secondary payload to map the lunar south pole for volatiles, especially water ice [20].

Other proposals are more focused on disruptive technology demonstration. For instance, a Cornell University student team is developing a lunar orbiter as part of NASA's Cube Quest Challenge. The proposed design consists on a water-based propelled Cubesat composed by two L-shaped halves that will split apart, gradually separate and continue its journey to the Moon [21].

Alternatively, there are other SmallSats prospective missions that focus on the potential of the Moon as a unique astronomical platform, especially the far side. This is particularly relevant for very low frequency radio astronomy from 0.3 MHz to 30 MHz, which represents a mostly unexplored band since Earth bound radio observations at these wavelengths are severely hampered by ionospheric distortions, man made interference, solar flares and even complete reflection below 10 MHz [22]. Therefore, it requires interferometric radio as-

tronomy from space. In this regard, *OLFAR* (Orbital Low Frequency ARray) aims to design a low-frequency distributed radio telescope in space using a large constellation of small spacecraft in orbit around the Moon. In order to reach that long term goal, two intermediate missions are being developed, *NCLE* and *CLE*. Netherlands-China Long-wavelength Explorer (*NCLE*) mission is expected to fly aboard the Chang'e-4 Satellite in 2018 and will demonstrate the performance of a first prototype of the radio-astronomy instrument based on network of nanosatellites; Cubesat Low frequency Explorer (*CLE*) aims at developing a concept for a trio of CubeSats that jointly perform an interferometric radio-astronomy mission [23].

Finally, several studies envisioning lunar cubesat constellations for communications and navigation purposes have emerged recently. Indeed, it is expected that future lunar exploration activities will combine robotic and human mission elements that should be able to communicate and support each other to advance in their operations and ultimately support a sustained human presence in the lunar environment [24]. For this, a lunar navigation and communication infrastructure, most likely be small spacecraft based, will be needed. For instance, Zhang and Wang [25] have presented a communications and navigation micro-satellite system concept to support future lunar south pole exploration missions. This relay and navigation satellite design is needed to effectively communicate and navigate with surface landers and rovers in these areas of the Moon since they have minimal to no direct access to Earth. As another example, Batista *et al* [26] have proposed a lunar Global Positioning System using CubeSats placed in a Rider constellation of two orbital planes. In this case, the recent advancements in chip-scale atomic clocks which can fit within the CubeSat platform act as a key enabler for this prospective low-cost lunar GPS that could make autonomous navigation on the Moon possible.

To conclude, although just some examples have been mentioned here, it is evident that lunar exploration is currently a key objective in the space community, mostly with the main long term goal of enabling future human missions to explore the Moon and then Mars. Cubesats represent a unique alternative for technology demonstration and scientific research that can help shorten the time and resources needed to achieve those long-term goals.

Chapter 3

State of the art

For decades, many efforts have been devoted to the quest for trajectories to transfer a spacecraft from the Earth to the Moon. Traditionally, the problem has been divided into two main categories: unlimited thrust orbit transfers or impulsive burn orbit transfers, modeled with zero burn time burns; and limited thrust or finite burn orbit transfers, which use a nonzero burn time [27]. This chapter will give an overview on the state of the art of Earth-Moon trajectory design. This is particularly relevant, since in this work we will be adapting some concepts coming precisely from the impulsive transfers literature and tailoring them to the sizing and propulsive constraints that characterize a Cubesat mission.

3.1 Impulsive burn orbit transfers

Concerning the impulsive burn orbit transfers, a Hohmann transfer orbit with the perigee on the Earth parking orbit and the apogee on the Moon orbit represents the simplest way to perform the Earth-Moon transfer and is illustrated in Figure 3.1.1a. The Hohmann transfer is a special case of the *patched conics approach*, where the mission is broken into phases that are connected by patches where each patch is the solution of a two body problem. This approach provides us with an analytic solution for the transfer, but it entails large ΔV maneuvers to inject the spacecraft into the final orbit around the Moon.

Alternatively, *low-energy transfers* emerged as a solution to reduce this high cost for Earth-Moon trajectories, making possible missions which classical approaches could not. Such trajectories are achieved by exploiting gravity as much as possible, using the natural dynamics arising from the presence of a third body (or more bodies). The term *low-energy* is used to refer to the low fuel and therefore low energy required to control the trajectory from a given starting condition to a targeted final condition [28]. Typically, Earth-Moon low energy transfers exploit the concept of temporary ballistic capture, or weak capture, which is defined in the framework of n-body problems. In this kind of transfers, the spacecraft is ballistically captured at the Moon, it is, no ΔV is required to reach the periapsis of an elliptic lunar orbit. Even though the time of flight is larger than the Hohmann time of flight, these transfers resulted in substantial propellant savings and offered extended launch

windows. In this context, Belbruno and Miller [29] described the weak stability boundary transfer, which was successfully demonstrated with the *rescue* of Japanese spacecraft *Hiten*, that arrived at the Moon in 1991.

Low energy transfers have been the subject of countless works and can be divided into interior and exterior transfers. The reader is referred to [30] for a detailed review on the taxonomy of low energy transfers.

In the exterior transfers, the spacecraft is injected into an orbit having the apogee at approximately four Earth–Moon distances. In this region, a small maneuver, combined with a favorable exploitation of the Sun gravity gradient, makes it possible to approach the Moon from the exterior, and to perform a lunar ballistic capture [29]. Exterior transfers can be also viewed from the perspective of Lagrangian points dynamics [28, 31]. In this sense, Koon, Marsden *et al* [28, 32] proposed a systematic procedure to reproduce a *Hiten*-like mission. This approach was based on approximating the Sun-Earth-Moon-spacecraft four body system with two three-body systems. In this way, one could exploit the invariant manifold structures of the Lagrange points of the three-body systems and construct Earth-Moon low energy transfer trajectories with ballistic capture at the Moon. The resulting transfers involved an initial impulsive ΔV to inject the spacecraft in the transfer trajectory, and another one at the patching point between the two three-body systems, as Figures 3.1.1b and 3.1.1c illustrate. Indeed, this method will be used in Section 5.1 in order to generate initial guess solutions for Cubesat Earth-Moon transfers.

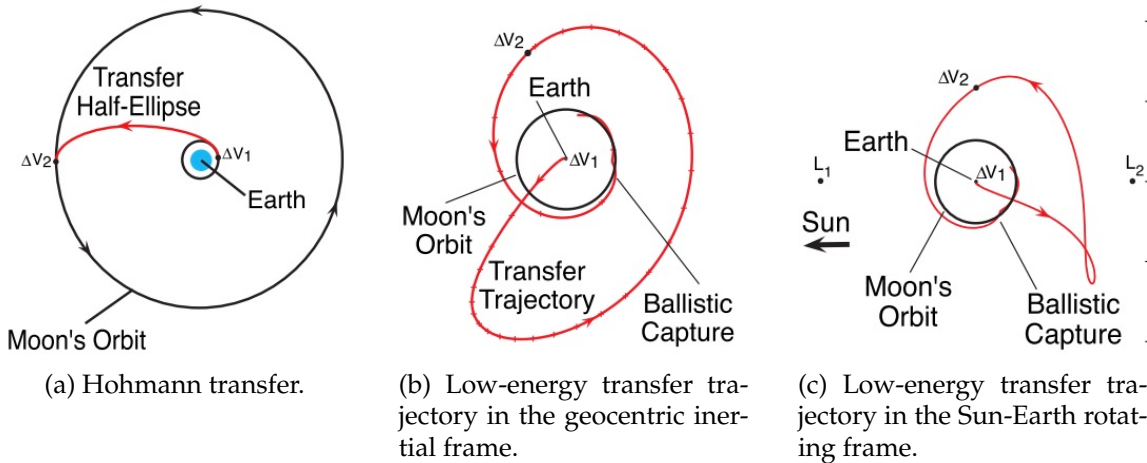


Figure 3.1.1: Different approaches to Earth-Moon transfers [28].

In the interior transfers, most of the trajectory is defined within the Moon orbit. These transfers exploit the dynamics of the cis-lunar region in the Earth–Moon system [33] with trajectories transitioning through the L_1 point and can be defined in the Earth-Moon restricted three-body problem since the solar perturbation is not crucial. Other kinds of interior transfers exploit the resonances between the transfer orbit and the Moon [30].

Up to now, we have introduced three main approaches to impulsive burn transfers: patched-conics, interior low-energy transfers, and exterior low-energy transfers. These trajectories are defined in the two-, three-, and four-body problems, respectively. In an attempt

to propose a common framework for these three approaches, a four-body model was proposed by Topputo [30] to optimize two-impulse Earth–Moon transfers with transfer duration lower or equal than 100 days, and extract the set of Pareto-efficient solutions starting from a common dynamical model. The problem was formulated with mathematical means and solved through direct transcription and multiple shooting strategy. Thousands of solutions were found and families of solutions were defined and characterized, and their features discussed. In Section 5.2, the methodology presented in [30] to span and search the solution space will be reproduced in order to obtain initial guesses for the Cubesat Earth–Moon transfer trajectories.

3.2 Limited burn orbit transfers

In this type of transfers, the thrust and acceleration magnitudes are bounded and the burn times are nonzero. One of the earliest approach to this kind of transfers was based on optimal trajectories that were geometrically similar to the impulsive solution counterparts [27, 34]. In this way, GS2BI (Geometrically Similar to the 2-Burn Impulsive) and GS3BI (Geometrically Similar to the 3-Burn Impulsive) trajectories were proposed, since it had been shown that minimum fuel impulsive trajectories required two or at most three burns.

In the 90s, Golan and Breakwell [35] proposed Earth–Moon transfers for power-limited spacecraft trajectories found by matching an Earth spiral to a Moon spiral at some intermediate distance, as depicted in Figure 3.2.1. Pierson and Kluever [36] solved minimum-fuel, three-dimensional trajectories from a circular LEO to an inclined circular LLO using optimization methods in the context of the classical restricted three-body problem and separating the problem in three-stages (thrust-coast-thrust). Herman and Conway [37] combined the method of collocation with nonlinear programming (NLP) to solve the transfer problem in the context of two coupled two-body problems taking into account the respective third-body disturbance accelerations of Earth and Moon.

Limited burn orbit transfers are generally associated to electric propulsion systems, since they are thrust-limited. In this regard, it has been demonstrated that the cost for low energy transfers (such as the ones described in the previous subsection) can be further reduced by using low-thrust propulsion [38, 39], since it is possible to reduce the propellant necessary to send a spacecraft to the Moon by exploiting both the simultaneous gravitational attractions of the Sun, the Earth, and the Moon, and the high specific impulse provided by the low-thrust engines (e.g., ion engines) [39]. A successful example of this approach was the mission SMART-1, which reached a selenocentric orbit by following a preset thrust profile equipped with only a single ion engine with a maximum thrust of 70 mN [40].

In this same line of thought, Betts and Erb [41] showed that direct transcription or collocation methods could be successfully applied to low-thrust Earth–Moon transfers. In [41], they presented low thrust electric propulsion transfers representative of the SMART-1 mission which took the spacecraft from an elliptic Earth centered parking orbit to a polar lunar elliptic orbit with pericenter above the south pole. The main drawback of this approach was that the solution space was constrained by dividing the trajectory into the three dis-

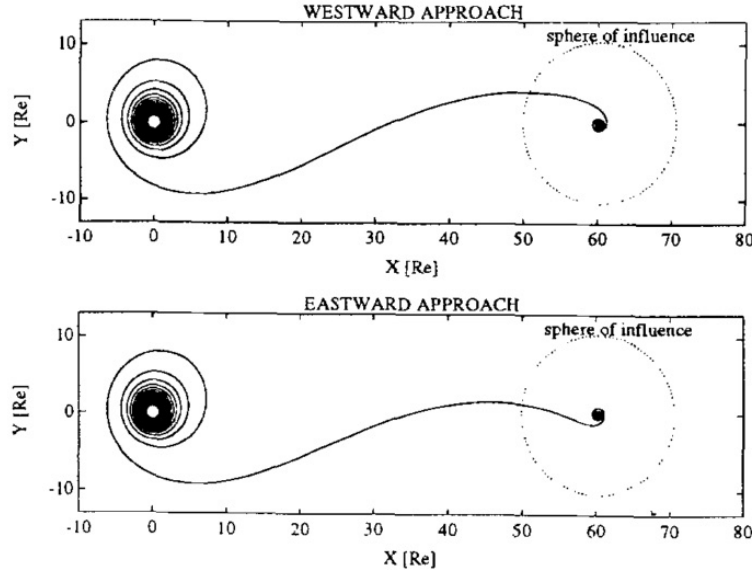


Figure 3.2.1: Lunar trajectories in the Earth-Moon rotating frame. Distance unit is the Earth radius, Re [35].

tinct phases illustrated in Figure 3.2.2, namely, geocentric burn, geocentric coast and selenocentric burn. The resulting transfers took over 200 days and it consisted in minimum fuel transfers using two burns (corresponding to phase 1 and phase 2). It was also stated that it is more fuel efficient to use many (short duration) burns than one long duration burn, however, this involves is a penalty in the time duration of the transfer. This multiple burn concept for SMART-1 was investigated in [42], where fuel efficient transfer trajectories were constructed without applying optimization techniques, combining low thrust and multiple Moon swing-by's. The transfer duration was about 17 months and the fuel demanded for a 350 kg launch mass ranged from 54.3 kg to 60.9 kg depending on the launch date. Alternatively, for the two-burn approach proposed in Betts and Erb [41], the optimal solution required 14-21 kg more of fuel but just 10.3 months of transfer duration.

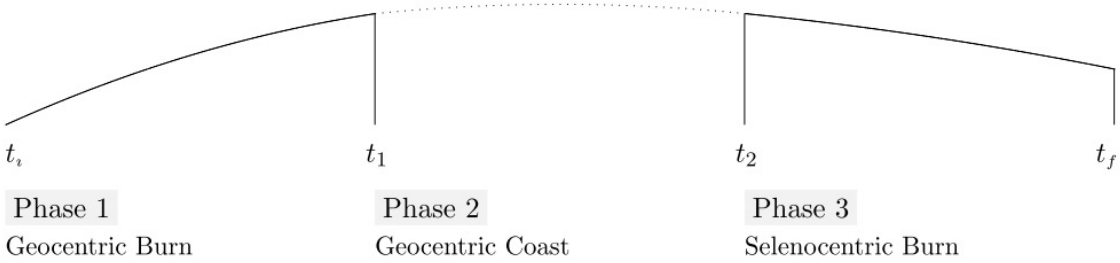


Figure 3.2.2: Earth-Moon transfer trajectory phases [41].

A different approach towards low-energy, low-thrust Earth-Moon transfers is the one adopted in [39,43]. Mingotti *et al* [39] proposed a low-thrust adaptation of the systematic ap-

proach detailed in [28] for the construction of Earth-Moon transfers based on the invariant manifolds associated to the collinear Lagrange points. In this case, the coupled restricted three-body problem approximation is used to deliver an appropriate first guess for the subsequent optimization of the transfer trajectory within a complete four-body model using a direct multiple shooting strategy. Although the initial guess generation follows different steps, Sullo *et al* [43] also relied in the multi-body dynamics and invariant manifolds to generate initial guesses to be later optimized using NLP. With Mingotti's [39] approach, an impulsive maneuver is carried out by the launch vehicle at the initial instant and this places the spacecraft on a translunar trajectory; from then on, the spacecraft is able to reach a stable orbit around the Moon relying just on its low thrust propulsion. Mingotti *et al* [39] presented transfers for a 1000 kg spacecraft with 0.5 N of maximum thrust from a 200 km altitude Earth circular orbit to an elliptic Moon orbit of 1000 km of periapsis and 10000 km of apoapsis, lasting over 200 days, with an initial impulsive ΔV of approximately 3 km/s and requiring between 3 and 6% of fuel with respect to the total initial mass.

Alternatively, Evolutionary Neurocontrol Methods (ENC) have been proposed in [40] to solve the planetary case of an Earth-Moon transfer. ENC is the application of Artificial Neural Networks (ANN), trained by Evolutionary Algorithms (EA), to compute optimal spacecraft steering [44]. This method, that has been already used for interplanetary low-thrust trajectory optimization, offers some advantages over direct transcription or collocation methods since it does not require a continuous fully valid initial guess solution and state derivatives and it does not require the problem to be split into different phases to achieve a globally optimal solution. Promising results for transfers from GTO to circular Moon orbit and from GTO to SMART-1 orbit were offered in [40]; the main disadvantage to this method's application being the limitation to a single SOI (Sphere Of Influence) crossing.

As it can be seen, Earth-Moon transfers have been studied for decades; in particular, the interest on low energy low thrust transfers has been increasing in the last years. Very recently, some mission analysis studies have appeared concerning Earth-Moon Cubesat transfers to the Moon. For instance, some research has been presented for JAXA's EQUULEUS, a 6 U Earth-Moon Lagrangian Point orbiter [45]. The need for the development of non-standard trajectories that allow for Cubesat low energy transfers is also recognized in [46] in the context of *The Vermont Space Grant Lunar Lander Project*.

Finally, Folta *et al* [47] used Purdue University and Goddard Space Flight Center's Adaptive Trajectory Design tool and dynamical system research to uncover cislunar spatial regions permitting viable Earth-Moon transfer arcs for the 6 U lunar icecube mission. Although using an alternative approach, the study in [47] somewhat pursues the same goal that the work presented in this thesis, which is to provide a design framework for Cubesats Earth-Moon transfers.

In conclusion, although some related work has started to emerge in the last years, the possibility of extrapolating traditional spacecraft transfers to Cubesats is mostly unexplored and will be the main object of study in this work, in which two different methods from the impulsive transfers literature are adapted to obtain initial guess Earth-Moon Cubesat transfer trajectories that will be later optimized for minimum fuel consumption.

Chapter 4

Background

The objective of this chapter is to explain in a concise way some dynamical concepts and models used throughout this work, with the aim to ease the understanding of the following sections. This is why it will not be an extensive review, it will instead be rather focused on the concepts that, in the writer's opinion, are necessary to comprehend the procedures and results presented, especially in Section 5.1.

4.1 Dynamic models

4.1.1 Planar Circular Restricted Three-Body Problem

The Circular Restricted Three-Body Problem (CR3BP) constitutes a well-known and very useful model to study the dynamic evolution of a particle P moving under the gravitational influence of two bodies, P_1 and P_2 , collectively referred to as the *primaries*, that have masses m_1 (primary mass) and m_2 (secondary mass). In this model, the primaries are assumed to move following circular orbits centered in their barycenter. Besides, the mass of P is assumed to be negligible with respect to m_1 and m_2 , so that its dynamics have no impact on the motion of the primaries. The general CR3BP is depicted in Figure 4.1.1.

If we further constrain the model so that particle P can only move in the plane defined by P_1 and P_2 orbits (planar motion), the complexity of the problem reduces while still being representative enough for many applications. Equations (4.1) to (4.4) describe the motion of P in the resulting Planar Circular Restricted Three-Body Problem (PCR3BP), where \bar{U} is the augmented or effective potential and r_1, r_2 are the distance of P to the primaries [28]. The equations are written with respect to the synodic reference frame, which is centered in the barycenter of P_1 and P_2 and rotates coherently with the primaries so that the X axis is always in the P_1 - P_2 direction. In this reference system, P_1 and P_2 are fixed in position, at $(-\mu, 0)$ and $(1 - \mu, 0)$, respectively, where $\mu = \frac{m_2}{m_1 + m_2}$ is the mass parameter and $\mu_1 = 1 - \mu$, $\mu_2 = \mu$.

$$\ddot{x} - 2\dot{y} = -\frac{\partial \bar{U}}{\partial x}, \quad \ddot{y} + 2\dot{x} = -\frac{\partial \bar{U}}{\partial y} \quad (4.1)$$

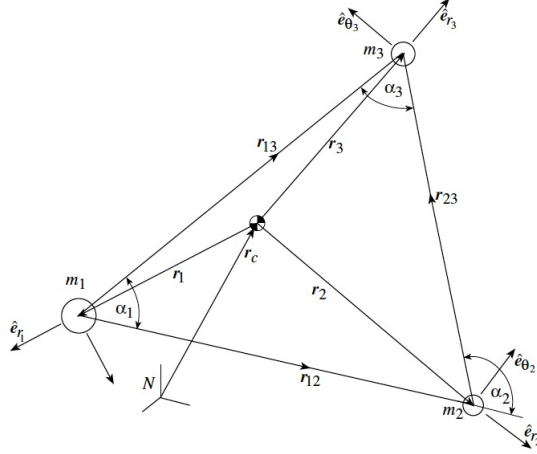


Figure 4.1.1: General configuration for the CR3BP [48].

$$\bar{U}(x, y) = -\frac{1}{2}(x^2 + y^2) + U(x, y) = -\frac{1}{2}(\mu_1 r_1^2 + \mu_2 r_2^2) - \frac{\mu_1}{r_1} - \frac{\mu_2}{r_2} \quad (4.2)$$

$$r_1 = \sqrt{(x + \mu_2)^2 + y^2} \quad (4.3)$$

$$r_2 = \sqrt{(x - \mu_1)^2 + y^2} \quad (4.4)$$

For simplicity, the equations have been normalized with the following characteristic magnitudes:

- $d = L\bar{d}$, where L is the distance between the primaries
- $t = \frac{T}{2\pi}\bar{t}$, where T is the orbital period of the primaries

Note that the equations of motion are written in terms of the gravitational potential U and the *effective* or *augmented* potential \bar{U} . Indeed, the motion is conservative in the synodic reference frame since all the forces that work can be written in potential form (Coriolis does not work because it is always perpendicular to the velocity vector).

Multiplying Equations (4.1) by the velocity components, adding them together, and integrating, we obtain the energy integral of motion, E :

$$\dot{x}\ddot{x} + \dot{y}\ddot{y} = \dot{r}\ddot{r} = -\dot{r} \cdot \nabla U \quad (4.5)$$

$$E(x, y, \dot{x}, \dot{y}) = \frac{1}{2}(\dot{x}^2 + \dot{y}^2) + \bar{U}(x, y) \quad (4.6)$$

Apart from E , it is very frequent to use as well what is called the *Jacobi integral*, given by:

$$C(x, y, \dot{x}, \dot{y}) = -(\dot{x}^2 + \dot{y}^2) - 2\bar{U}(x, y) \quad (4.7)$$

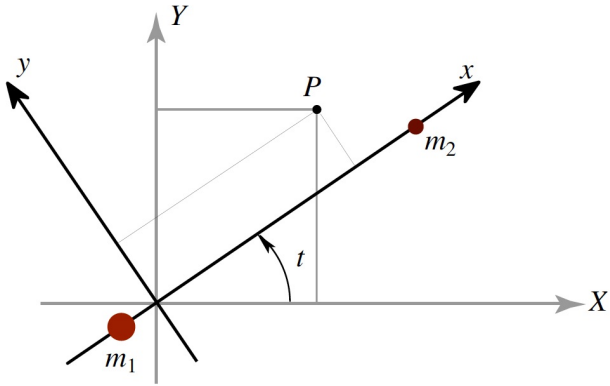


Figure 4.1.2: Inertial and rotating frames in the CR3BP. The rotating coordinate system with coordinates x and y moves counterclockwise with unit angular velocity relative to the inertial frame with coordinates X and Y [28].

Although it may seem that this model is too simple to be used to describe the motion of subsystems of the solar system, it has proved to be very useful in providing an understanding of a wide range of dynamical behaviors. The hierarchy of masses in the solar system and the low eccentricities of most of the planets' orbits are some of the reasons why the CR3BP or even the PCR3BP are widely used to obtain a simple yet good approximation for certain systems, especially for the qualitative behavior [28].

In this work, the PCR3BP will be applied to the Earth-Moon-Spacecraft and the Sun-Earth-Spacecraft systems separately, which has proved to be very useful to determine initial guess trajectories for Earth-Moon transfers. This model is not fully realistic since the Moon and Earth motion is not completely circular nor planar. However, the approximation is accurate enough for the purpose of generating an initial guess since the Moon orbit's inclination is just 5° with respect to the ecliptic and the orbit eccentricity is 0.0549.

Realms of possible motion

In the PCR3BP, the state is defined in a four-dimensional space defined by (x, y, \dot{x}, \dot{y}) . In the same way, each value e of the energy integral E defines a three-dimensional subset of that four-dimensional phase space, which is called an *energy surface*, defined in Equation (4.8).

$$\mathcal{M}(\mu, e) = \{(x, y, \dot{x}, \dot{y}) \mid E(x, y, \dot{x}, \dot{y}) = e\} \quad (4.8)$$

The projection of this surface onto position space in the rotating frame (x - y plane) is called the Hill's Region, and it is the region of possible motion for a particle P with energy level e , defined in Equation (4.9). The boundary of $\mathcal{M}(\mu, e)$ is known as the *zero velocity*

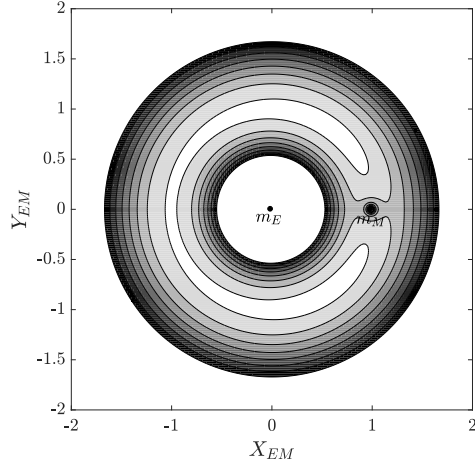


Figure 4.1.3: Zero-velocity contours of the Earth-Moon system.

curve because the velocity and kinetic energy of a particle in this curve are zero, and so the particle can only move on the side of the curve where the kinetic energy is positive. In the other side, the kinetic energy would be negative, which is infeasible and therefore it represents a *forbidden region of motion* [28]. Note that when a particle is located on this surface, this implies only that its velocity relative to the rotating frame is zero, not that its inertial velocity is zero [48].

$$M(\mu, e) = \{(x, y) \mid \bar{U}(x, y,) \leq e\} \quad (4.9)$$

Figure 4.1.3 shows selected zero-velocity contours for the Earth-Moon system. The darker the color, the greater the energy (relative to the synodic frame) that is needed to enter those areas.

Finally, Figure 4.1.4 shows five different configurations for the realms of possible motion for a given μ , which in this example coincides with the one associated to the Earth-Moon system. A particle with each given value of energy would be able to move through the white areas but the shaded ones would be forbidden. These five configurations are delimited (in terms of energy) by the zero-velocity energy levels of the libration points of the system, that we will discuss in the next section.

Equilibrium points

For practical purposes, we can easily rewrite Equations (4.1) in first-order form, obtaining Equations (4.10). Then, in order to find the equilibrium points, it will be enough to set the right-hand sides of the equations to zero.

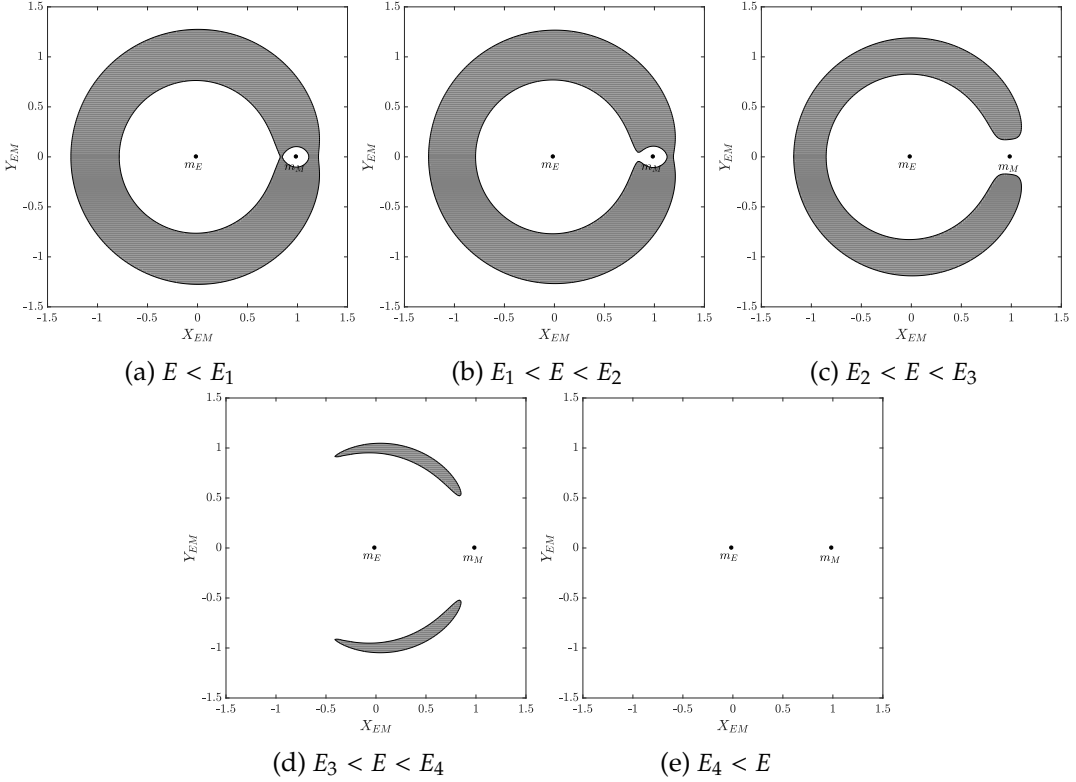


Figure 4.1.4: Realms of possible motion for five different energy levels. The shaded gray areas corresponds to the forbidden realm.

$$\begin{aligned}
 \dot{x} &= v_x \\
 \dot{y} &= v_y \\
 \dot{v}_x &= 2v_y - \frac{\partial \bar{U}}{\partial x} \\
 \dot{v}_y &= -2v_x - \frac{\partial \bar{U}}{\partial y}
 \end{aligned} \tag{4.10}$$

The PCR3BP admits five different equilibrium points which are normally known as the *Lagrangian libration points* or simply *Lagrange points*. Three of them are collinear and located on the x-axis and are referred to as L_1 , L_2 and L_3 . The two left form two equilateral triangles with the primaries and are called L_4 and L_5 . For clarity, the five Lagrange points for the Earth-Moon system are depicted in Figure 4.1.5.

In this work we are specially interested in the collinear Lagrange points, since we will exploit the dynamics around those points, particularly L_2 , to achieve more efficient transfers to the Moon. First of all, in order to compute those points, we particularize the Equation $\dot{v}_x = 0$ for $y = 0$. Since $v_y = 0$ at equilibrium, finding the collinear equilibrium points reduces to finding $\bar{U}_x = 0$, which translates into solving Equation (4.11), where γ_i is the distance of

L_i (L_1 or L_2) to the smallest primary and the upper and lower signs correspond to γ_1 and γ_2 , respectively.

$$\gamma^5 \mp (3 - \mu)\gamma^4 + (3 - 2\mu)\gamma^3 - \mu\gamma^2 \pm 2\mu\gamma - \mu = 0 \quad (4.11)$$

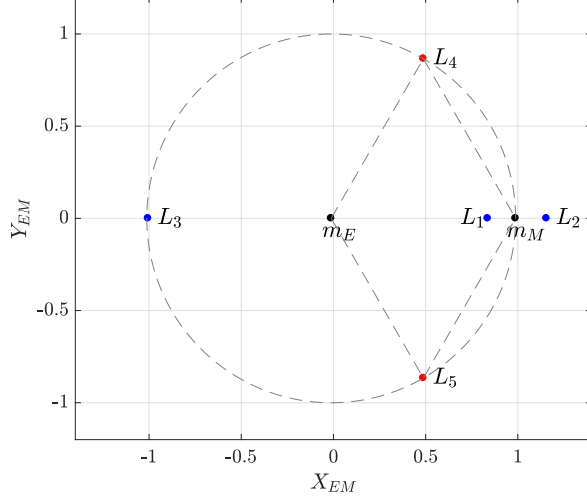


Figure 4.1.5: Lagrange points for the Earth-Moon PCR3BP.

Linearization near the collinear equilibrium points

The set of Equations (4.1) can be linearized around the collinear equilibrium points, L_1 and L_2 , which are of the form $(x_e, 0)$, yielding Equations (4.12).

$$\begin{aligned} \dot{x} &= v_x \\ \dot{y} &= v_y \\ \dot{v}_x &= 2v_y + ax \\ \dot{v}_y &= -2v_x - by \end{aligned} \quad (4.12)$$

where $a = 2\bar{\mu} + 1$ and $b = \bar{\mu} - 1$ and $\bar{\mu} = \mu / |x_e - 1 + \mu|^{-3} + (1 - \mu) / |x_e + \mu|^{-3}$. This linearization is very useful to study the PCR3BP dynamics in the vicinity of the libration points, which will be key to define itineraries between the different realms of motion, as it will become evident in Section 5.1.

4.1.2 Planar Bicircular Restricted Four-Body Problem

There are, however, systems in which the PCR3BP falls short and it is not representative enough for our purposes, since the system is heavily affected by the perturbation of a third primary, P_3 . Maintaining the constraints regarding the circular character of the orbits and

the planar configuration of the PCR3BP but adding this P_3 perturbation, the Planar Bicircular Restricted Four Body Problem (PBRFBP) is obtained. In this case, we are interested in the Sun-Earth-Moon-Spacecraft four body problem. Equations (4.13) to (4.16) correspond to the equations of motion of this particular PBRFBP, which are written in a rotating coordinate system centered on the Earth-Moon barycenter, illustrated in Figure 4.1.6. The model is not physical, since the motion is not completely coherent: all primaries are assumed to move in circular orbits. However, it serves as a good enough representation of the real four-body dynamics for our purposes. Indeed, the eccentricities of the Earth and Moon orbits are just 0.0167 and 0.0549, while the Moon orbit inclination is only 5° from the ecliptic. The reader is referred to [30, 49] for further details on the model.

$$\ddot{x} - 2\dot{y} = \frac{\partial \Omega_4}{\partial x}, \quad \ddot{y} + 2\dot{x} = \frac{\partial \Omega_4}{\partial y} \quad (4.13)$$

$$\Omega_4(x, y, t) = \Omega_3(x, y) + \frac{m_s}{r_3(t)} - \frac{m_s}{\rho^2}(x \cos(\omega_s t) + y \sin(\omega_s t)) \quad (4.14)$$

$$\Omega_3(x, y) = \frac{1}{2}(x^2 + y^2) + \frac{1-\mu}{r_1} + \frac{\mu}{r_2} + \frac{1}{2}\mu(1-\mu) \quad (4.15)$$

$$r_3 = [(x - \rho \cos(\omega_s t))^2 + (y - \rho \sin(\omega_s t))^2]^{1/2} \quad (4.16)$$

where $m_s = 3.28900541 \cdot 10^5$ is the scaled mass of the Sun, $\rho = 3.88811143 \cdot 10^2$ is the scaled Sun-(Earth+Moon) distance, $\omega_s = -9.25195985 \cdot 10^{-1}$ is the scaled angular velocity of the Sun and $\mu = 1.21506683 \cdot 10^{-2}$ is the Earth-Moon mass parameter.

In this model, the equations have been made non-dimensional using the following characteristic magnitudes:

- Characteristic length, $LU = 3.84405000 \cdot 10^8$ m, corresponds to the distance between the Earth and the Moon.
- Characteristic time, $TU = \frac{T}{2\pi} = 4.34811305$ days, where T corresponds to the Earth-Moon orbital period.
- Characteristic mass, $MU = 6.0458 \cdot 10^{24}$ kg, corresponds to the addition of the Earth and Moon masses.

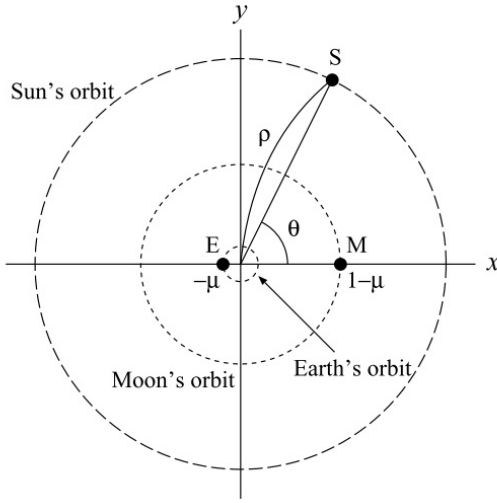


Figure 4.1.6: Rotating coordinate system. The positions of the Earth (E), Moon (M) and Sun (S) are depicted. The short-dashed circles represent the Earth's and Moon's orbits in the non- rotating coordinate system, and long-dashed circle represents the Sun's orbit in the rotating coordinate system [49].

4.1.3 Transforming coordinates between rotating frames

This section is based on [28] and will present a general procedure to transform coordinates between two rotating frames. In this work, this has been particularly useful to transform states from the Sun-Earth-Spacecraft three body system to the Earth-Moon-Spacecraft system and viceversa. Namely, the transformation will imply two rotations and also scaling, since the characteristic magnitudes used to normalize the equations are different for the two reference systems.

In this way, imagine we have the coordinates of particle P expressed in and with respect to rotating reference system A and we want to express them with respect to another rotating reference frame, B.

Transformation from synodic system A to an inertial reference frame The first step is to transform the coordinates to the inertial system centered on one of the primary masses of system A, namely, m_1 or m_2 . For that, we will use Equation (4.17).

$$x_A^{\text{in}} = R(x_A^{\text{rot}} - d_A) \quad (4.17)$$

where R is the rotation matrix defined in (4.18) and $d_A = [x_{A'}^0, 0, 0, 0]^T$, x_A^0 being the distance from the origin of the synodic frame A to the primary mass on which the inertial reference system is centered, meaning that x_A^0 will be $-\mu_A$ or $1 - \mu_A$ depending on whether the inertial reference system is centered on m_1 or m_2 .

$$R = \begin{pmatrix} R_{11} & 0 \\ R_{21} & R_{22} \end{pmatrix} \quad (4.18)$$

$$R_{11} = R_{22} = \begin{pmatrix} c & -s \\ s & c \end{pmatrix}, \quad R_{21} = \begin{pmatrix} -s & -c \\ c & -s \end{pmatrix} \quad (4.19)$$

$$c = \cos(\theta(t_A)), \quad s = \sin(\theta(t_A)) \quad (4.20)$$

Units scaling The next step is to change the scaling of the states and times due to the difference in the characteristic magnitudes with which systems A and B are normalized, according to Equations (4.21), (4.22) and (4.23).

$$x_B^{\text{in, pos}} = \frac{L_A}{L_B} x_A^{\text{in, pos}} \quad (4.21)$$

$$x_B^{\text{in, vel}} = \frac{L_A}{L_B} \frac{T_B}{T_A} x_A^{\text{in, vel}} \quad (4.22)$$

$$t_B = \frac{T_A}{T_B} t_A \quad (4.23)$$

Transformation from the inertial reference frame to synodic system B Finally, we perform a transformation similar to the one explained in the first step, but in this case, we are going from an inertial system to a synodic one. For that, we use Equation (4.24):

$$x_B^{\text{rot}} = R^{-1} x_B^{\text{in}} + d_B \quad (4.24)$$

where $d_B = [x_B^0, 0, 0, 0]^T$ and x_B^0 is $-\mu_B$ or $1 - \mu_B$ depending on the primary mass on which reference system B is centered on.

4.2 Invariant manifolds theory

In this work, we will exploit the *N-body dynamics*, particularly the invariant manifolds of the periodic orbits of the L_2 libration point in the PCR3BP. This section will provide the necessary background on dynamical systems in a concise way in order to properly understand the concepts in Section 5.1. For more detail, the reader is referred to [50] and [51].

In a general way, let us consider an autonomous dynamical system with two degrees of freedom, defined by the set of differential equations below:

$$\begin{aligned} \ddot{x}_1 &= F_1(x_1, x_2, \dot{x}_1, \dot{x}_2) \\ \ddot{x}_2 &= F_2(x_1, x_2, \dot{x}_1, \dot{x}_2) \end{aligned} \quad (4.25)$$

The initial conditions are defined as $(x_{10}, x_{20}, \dot{x}_{10}, \dot{x}_{20})$ and the solution has the form $x_1(x_{10}, x_{20}, \dot{x}_{10}, \dot{x}_{20}; t)$ and $x_2(x_{10}, x_{20}, \dot{x}_{10}, \dot{x}_{20}; t)$. Let us assume the solution of the system is periodic with period T , meaning that $x_i(x_{10}, x_{20}, \dot{x}_{10}, \dot{x}_{20}; t + T) = x_i(x_{10}, x_{20}, \dot{x}_{10}, \dot{x}_{20}; t)$.

In this case, we are interested in studying the behaviour of the system in the vicinity of this periodic solution. For that, we can rewrite the system of Equations (4.25) in first order form, obtaining Equations (4.26), or in general, Equation (4.27). Let $x_i = x_i(x_{10}, x_{20}, \dot{x}_{10}, \dot{x}_{20})$, ($i = 1,..4$) be a solution of the system. Then, we consider slightly perturbed initial conditions, with a perturbation $\xi_i(0)$ small enough so that the new solution can be expressed as in Equation (4.28) [50].

$$\begin{aligned}\dot{x}_1 &= x_3 \\ \dot{x}_2 &= x_4 \\ \dot{x}_3 &= F_1(x_1, x_2, x_3, x_4) \\ \dot{x}_4 &= F_2(x_1, x_2, x_3, x_4)\end{aligned}\tag{4.26}$$

$$\dot{x}_i = f_i(x_1, x_2, x_3, x_4), \quad i = 1,..4\tag{4.27}$$

$$x'_i(t) = x_i(t) + \xi_i(t), \quad i = 1,..4\tag{4.28}$$

Since $\xi_i(0)$ is small, we can assume $\xi_i(t)$ is small as well, at least for a finite time interval. Then, we can substitute the perturbed solution (Equation (4.28)) into the system of differential Equations (4.27) and linearize it to first order terms in $\xi_i(t)$, obtaining the system of *variational equations*:

$$\dot{\xi}_i = \sum_{k=1}^4 p_{ik} \xi_k, \quad p_{ik} = \left(\frac{\partial f_i}{\partial x_k} \right)_{x_i(t)}, \quad i = 1,..4\tag{4.29}$$

The general solution of system of Equations (4.29) is a linear combination of four linearly independent solutions which can be arranged in what is called the *fundamental matrix of solutions*, ϕ , so that the general solution of the variational equations takes the form:

$$\xi(t) = \phi(t) \xi(0)\tag{4.30}$$

It can be shown that if the solution $x(t)$ is periodic, then the system of variational equations corresponding to this periodic solution is a linear system with periodic coefficients. Then, for $t = T$ or more generally, for $t = nT$, the following equations hold:

$$\begin{aligned}\xi(T) &= \phi(T) \xi(0) \\ \xi(nT) &= [\phi(T)]^n \xi(0)\end{aligned}$$

The matrix $\phi(T)$ is called the *monodromy matrix*. These equations provide the evolution of the perturbed orbit $x'(t)$ with respect to the unperturbed one $x(t)$. It is clear then that

the stability of $x'(t)$ depends on the evolution of $\xi(t)$ and therefore on the eigenvalues of the monodromy matrix, which are called *Floquet multipliers*. Then, if all Floquet multipliers satisfy $|\lambda| \leq 1$, the system is stable. In other words, for the system to be stable, all Floquet multipliers must lie inside the unitary circle in the complex plane.

In this work, we are particularly interested in the dynamical behavior in the vicinity of the CR3BP libration point periodic orbits. In this problem, the variational equations are Equations (4.12) and all the concepts explained above for a general system hold perfectly for this particular case. Besides, it can be shown that for planar Lyapunov orbits in the PCR3BP the four eigenvalues of the monodromy matrix include one real pair and one pair equal to unity:

$$\lambda_1 > 1, \quad \lambda_2 = \frac{1}{\lambda_1}, \quad \lambda_3 = \lambda_4 = 1$$

The aforementioned libration point periodic orbits of the PCR3BP have an associated set of *invariant manifolds*, which are trajectories that asymptotically depart or approach an orbit [52]. The unstable manifold W^U includes the set of all possible trajectories that a particle on a nominal orbit could traverse if it was perturbed in the direction of the orbit's unstable eigenvector, which is the one associated to the real and greater-than-1 eigenvalue. In other words, the unstable manifold contains all of the trajectories that exponentially depart the nominal orbit as time moves forward. On the other hand, the stable manifold W^S includes the set of all possible trajectories that a particle could take to arrive onto the nominal orbit along the orbit's stable eigenvector, which is the one associated to the smaller-than-1 eigenvalue. In this way, the stable manifold contains all of the trajectories the particle could take to exponentially depart the nominal orbit as time moves backwards. Figure 4.2.1 illustrates this discussion. Note also that each orbit has two associated stable and unstable manifold sets: one corresponding to a positive perturbation, and one corresponding to a negative perturbation.

It is worth mentioning as well that the manifolds have the physical property that all motion through the *bottleneck* in which the periodic orbit resides must occur through the interior of the manifold tubes, meaning that particles with initial conditions interior to a given manifold are guaranteed to move from one realm to another when evolved forward or backward in time. This means that we can define trajectories with prescribed itineraries by exploiting these manifold tube dynamics.

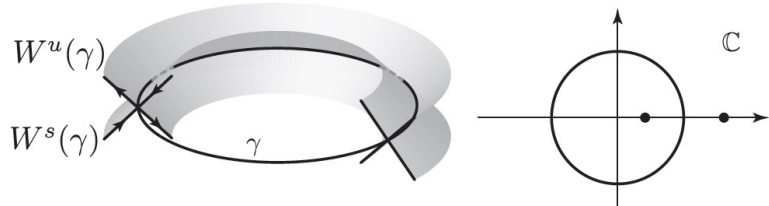


Figure 4.2.1: Stable and unstable manifolds of a periodic orbit whose monodromy matrix has one eigenvalue inside and one outside the unit circle [51].

Chapter 5

Initial Guess Construction

In this chapter, the initial guess construction process will be thoroughly explained. This is a critical step for the trajectory optimization scheme, since without a good guess, optimizers are likely to be unable to produce a good solution. In this work, two different trajectory design methods inherited from the impulsive transfers literature are used to find initial guesses for the Cubesat Earth-Moon transfers.

5.1 Initial Guess based on the invariant manifolds of the Lagrange points

This work will follow the systematic approach given in [28] to build low-energy transfer orbits from the Earth to the Moon relying on the theory of the invariant manifolds of the Lagrange points of both the Sun-Earth and the Earth-Moon systems. These trajectories will serve as initial guesses for the subsequent optimization detailed in Chapter 6. The underlying theoretical concepts supporting the following description can be found in Chapter 4.

In this approach, the transfer trajectory can be divided into two sections: the Earth escape leg and the Moon capture leg. For simplicity, and in order to be able to get the advantage of the known dynamical behavior related to the invariant manifolds of the Lagrange points, each leg will be modeled as in the Planar Circular Three-Body Problem. In this way, the Earth escape leg will be analyzed in the Sun-Earth-Spacecraft system, while the Moon capture leg will be studied in the Earth-Moon-Spacecraft system. Then, both legs will be connected at a patching point.

The transfer trajectory will start from a GEO orbit. Although Cubesats have been traditionally launched as secondary payloads into LEOs, launch opportunities have emerged to take small spacecraft as secondary payloads to GEOs, for example through Spaceflight Services, a company that works with Launch Services Providers including SpaceX, Orbital Sciences, Virgin Galactic, Kosmotras (Dnepr), and Progress (Soyuz). Therefore, for small spacecraft travelling to the Moon, starting in a GEO orbit is a reasonable assumption which also implies a significant reduction in time and propellant compared to LEO [53].

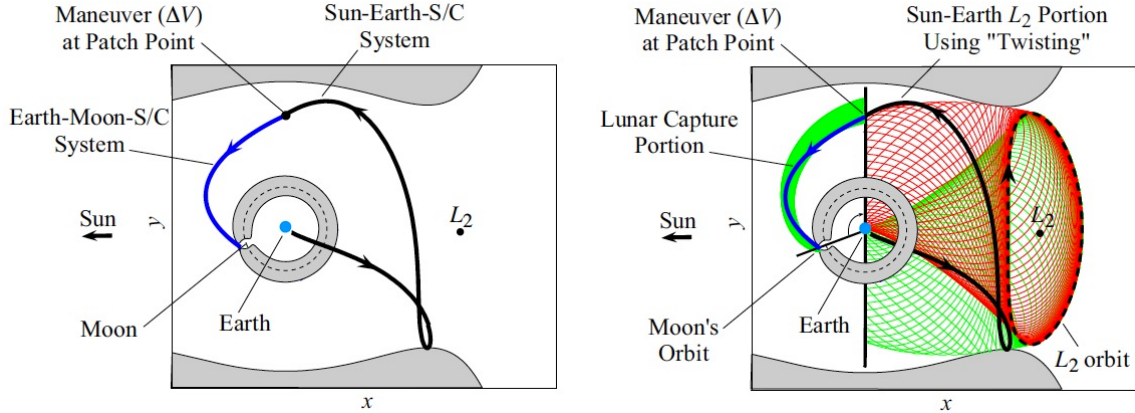


Figure 5.1.1: Sketch of the desired initial guesses to be obtained based on the dynamics of the invariant manifolds [28]. (—) Earth-Moon leg, (—) Sun-Earth leg.

At the initial instant, the launcher upper stage will provide a ΔV that will insert the spacecraft into a trajectory towards the Moon. In order for that trajectory to be *almost* ballistic, the concept of *orbit twisting* will be used to shape that trajectory so that the spacecraft starts the transfer following the Sun-Earth's L_2 stable manifold and then it *twists* to follow the Sun-Earth's L_2 unstable manifold which will intersect the same patching section as the Moon-Earth stable L_2 manifold. An sketch of the desired trajectory is presented in Figure 5.1.1.

5.1.1 Manifolds construction

As it has been already mentioned, this initial guess follows a prescribed path following the Sun-Earth and Earth-Moon Lagrange manifolds. At a later stage, the trajectories constructed in the Earth-Moon and in the Sun-Earth systems are patched by examining the intersection of the manifolds phase space in a given section. This is why obtaining the stable and unstable manifolds of both systems is the first step towards the initial guess construction. For that, we will heavily rely on the Invariant Manifolds theory presented in Section 4.2.

The procedure will be detailed here, presenting in parallel the results coming from both the Earth-Moon and Sun-Earth systems. The main steps in this process are the following: computation of the location of the collinear libration points, computation of periodic orbits around the libration points, and globalization of the stable and unstable manifolds.

In this section, non-dimensional units will be used coherently with the ones presented in Section 4.1.1. Table 5.1.1 gathers the values of those characteristic magnitudes for the two systems considered. The suffix used in the figures will indicate the system according to which the magnitude has been made non-dimensional, for instance, $X_{EM} = \frac{X}{L_{EM}}$.

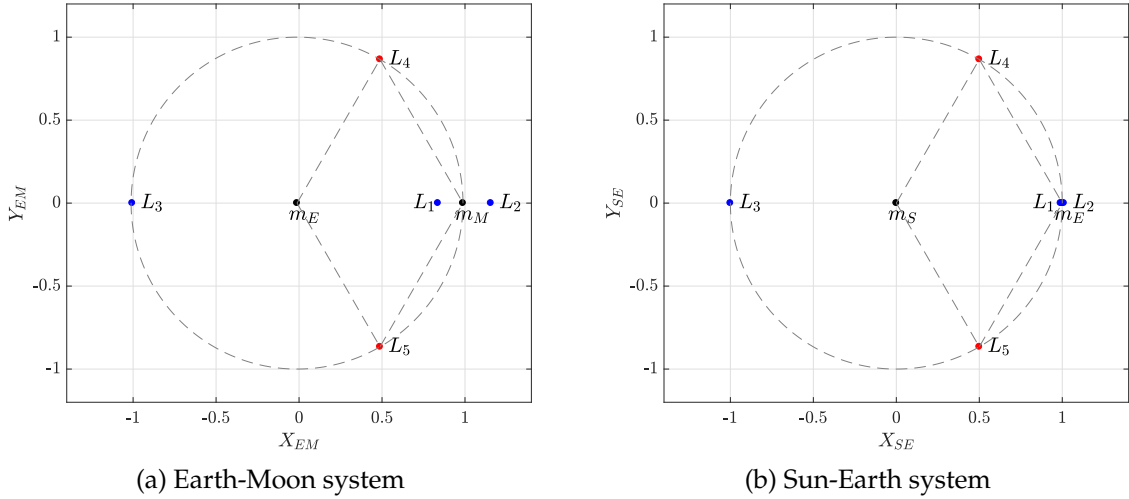
1. Computation of the location of the collinear libration points

For this step, we followed the procedure outlined in Section 4.1.1. Figure 5.1.2 depicts

Characteristic magnitude	Sun-Earth System	Earth-Moon System
L	$1.496 \cdot 10^8$ km	$3.85 \cdot 10^5$ km
$T/(2\pi)$	$3.156 \cdot 10^7/(2\pi)$ s	$2.361 \cdot 10^6/(2\pi)$ s

Table 5.1.1: Characteristic magnitudes for the PCR3BP Sun-Earth and Earth-Moon systems.

the results for the two systems considered.

Figure 5.1.2: Location of the libration points. (—) Collinear libration points, (—) Equilateral libration points, m_E , m_M and m_S refer to the Earth, Moon and Sun masses, respectively.

Concerning the energy levels, since the desired trajectory will need to travel through the L_2 necks of both the Earth-Moon and Sun-Earth systems, we need to compute the energy levels associated with the L_2 Lagrange points to make sure that the periodic orbit and the subsequent manifold can travel through that neck. According to Figure 4.1.4, this means $E > E_2$.

2. Computation of periodic orbits around the libration points

In order to obtain periodic orbits around the libration points, we need to work with the linearized dynamics around those points presented in Section 4.1.1 and solve an eigenvalue problem. The goal in this case is to use the linearized system of equations to find those initial conditions such that when integrated with the full non-linear PCR3BP system of equations, will lead to a periodic orbit around the libration point.

If we rewrite Equations (4.12) in matrix form, we arrive at the system in Equation (5.1).

$$\begin{pmatrix} \dot{x} \\ \dot{y} \\ \dot{v}_x \\ \dot{v}_y \end{pmatrix} = \begin{pmatrix} 0 & 0 & 1 & 0 \\ 0 & 0 & 0 & 1 \\ a & 0 & 0 & 2 \\ 0 & -b & -2 & 0 \end{pmatrix} \begin{pmatrix} x \\ y \\ v_x \\ v_y \end{pmatrix} \quad (5.1)$$

The characteristic polynomial of the linearized equations is the one in Equation (5.2), where $\bar{\mu}$ is the one defined in Section 4.1.1.

$$p(\beta) = \beta^4 + (2 - \bar{\mu})\beta^2 + (1 + \bar{\mu} - 2\bar{\mu}^2) \quad (5.2)$$

This polynomial has four different roots that are the eigenvalues of the system. Two of those eigenvalues are pure imaginary and conjugate numbers; the other two are two real numbers with the same absolute value and opposite sign.

On the other hand, it is well known that the general solution for a system like the one in Equation (5.1) (expressed in a concise way in Equation (5.3)) is the exponential one in Equation (5.4).

$$\dot{y} = Ay, \quad y(0) = y_0 \quad (5.3)$$

$$\dot{y} = y_0 e^{At} = \sum_{i=1}^4 c_i v_i e^{\beta_i t} \quad (5.4)$$

where suffix i identifies the corresponding eigenvector-eigenvalue pair (v, β) . As it can be seen, in order for the solution to be a purely periodic orbit, only the eigenpairs with the purely imaginary eigenvalues should be selected. This *selection* can be performed by choosing appropriate values for the constants c_i so that they are consistent with the initial conditions. In that way, in order to get a purely periodic orbit, the constants multiplying the two elements of the summation associated with the real eigenvalues, it is, $(c_{\mathbb{R}^+}, c_{\mathbb{R}^-})$, should be set to zero. Then, in order for the solution of the system dynamics to be real, the constants associated to the purely imaginary eigenvalues have to be constrained to be equal, $c_{\mathbb{I}^+} = c_{\mathbb{I}^-} = c_{\mathbb{I}}$.

For simplicity, we will choose our initial position to be placed on the x -axis, at a distance x_0 from the libration point, which is the *zero* for the linearized system. At this point, we expect the velocity of the periodic orbit to be directed in the y direction, therefore we can assume $v_{x_0} = 0$. If we particularize now Equation (5.4) at time $t = t_0 = 0$ we arrive at Equation (5.5) that reduces to Equation (5.6) once we take into account the aforementioned constraints. In this way, we can easily solve for $c_{\mathbb{I}}$ and v_{y_0} .

$$\begin{pmatrix} x_0 \\ y_0 \\ v_{x_0} \\ v_{y_0} \end{pmatrix} = c_{\mathbb{R}^+} \begin{pmatrix} v_{\mathbb{R}^+,1} \\ v_{\mathbb{R}^+,2} \\ v_{\mathbb{R}^+,3} \\ v_{\mathbb{R}^+,4} \end{pmatrix} + c_{\mathbb{R}^-} \begin{pmatrix} v_{\mathbb{R}^-,1} \\ v_{\mathbb{R}^-,2} \\ v_{\mathbb{R}^-,3} \\ v_{\mathbb{R}^-,4} \end{pmatrix} + c_{\mathbb{I}^+} \begin{pmatrix} v_{\mathbb{I}^+,1} \\ v_{\mathbb{I}^+,2} \\ v_{\mathbb{I}^+,3} \\ v_{\mathbb{I}^+,4} \end{pmatrix} + c_{\mathbb{I}^-} \begin{pmatrix} v_{\mathbb{I}^-,1} \\ v_{\mathbb{I}^-,2} \\ v_{\mathbb{I}^-,3} \\ v_{\mathbb{I}^-,4} \end{pmatrix} \quad (5.5)$$

$$\begin{pmatrix} x_0 \\ 0 \\ 0 \\ v_{y_0} \end{pmatrix} = c_{\mathbb{I}} \left[\begin{pmatrix} v_{\mathbb{I}^+,1} \\ v_{\mathbb{I}^+,2} \\ v_{\mathbb{I}^+,3} \\ v_{\mathbb{I}^+,4} \end{pmatrix} + \begin{pmatrix} v_{\mathbb{I}^-,1} \\ v_{\mathbb{I}^-,2} \\ v_{\mathbb{I}^-,3} \\ v_{\mathbb{I}^-,4} \end{pmatrix} \right] \quad (5.6)$$

At this point, we have the initial conditions for the desired periodic orbit around L_2 . If we were to numerically integrate these conditions in the linearized system of equations (Equations (4.12)), we would indeed obtain such periodic orbit. However, our goal is to obtain periodic orbits in the full non-linear system of equations (Equations (4.1)) as well. For that, the following procedure was used:

- (a) Numerically integrate Equations (4.1) starting at x_0 until the first X-axis crossing. The time it takes the dynamics to reach this point serves as an estimation of the desired Lissajous orbit's half period.
- (b) Apply a differential correction algorithm using as input the orbital period estimation and the initial conditions. In this case, an algorithm developed at the Department of Aerospace Engineering of University Carlos III of Madrid was used for this purpose. This algorithm outputs the corrected initial conditions and period for the periodic orbit to be coherent with the complete PCR3BP dynamics.
- (c) The procedure above is only valid for small amplitude periodic orbits around L_2 , since it is where the linearized equations hold and the guess for the initial condition is accurate enough for the differential correction algorithm to converge. In order to obtain larger orbits, a continuation method was used based on the orbital period; it is, a logic was used so that at each iteration the input to the algorithm in step (b) were the corrected initial conditions coming from the previous iteration together with the period obtained in the previous iteration plus a differential increase.

Figure 5.1.3 shows examples for the obtained periodic orbits for both the Sun-Earth and the Earth-Moon systems following the procedure detailed above.

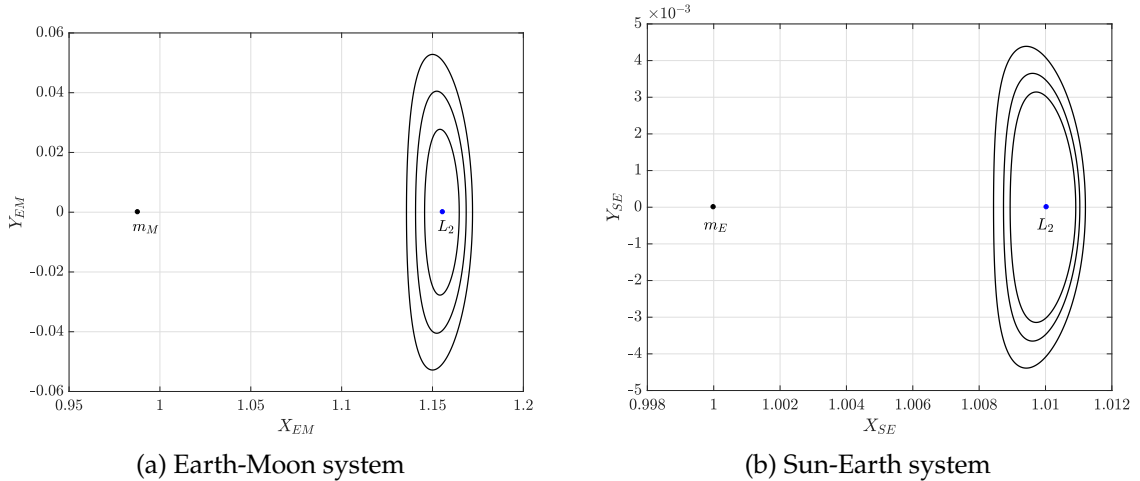


Figure 5.1.3: Examples of L_2 periodic orbits of different amplitude.

3. Globalization of the stable and unstable manifolds

The first step to obtain the invariant manifolds associated to the periodic orbit is to compute the state transition matrix, Φ , of the variational equations (Equations (4.12)).

This is done using Equation (5.7), where ϕ is the *fundamental matrix solution*.

$$\Phi(t) = \phi(t)\phi^{-1}(0) \quad (5.7)$$

Then, for a given set of points and times along the periodic orbit, we need to compute the eigenvalues and eigenvectors of the state transition matrix. From Section 4.2, we know that in the case of planar periodic orbits in the PCR3BP, those eigenvalues will include two real and reciprocal numbers together with two other eigenvalues equal to unity. These eigenvalues are also called *Floquet multipliers*.

$$\lambda_1 > 1, \quad \lambda_2 = \frac{1}{\lambda_1}, \quad \lambda_3 = \lambda_4 = 1$$

The eigenvector associated to λ_1 will be the unstable eigenvector, V^S , and the one associated to λ_2 will be the stable one, V^U . They will be used to compute the initial guesses for the unstable and stable manifolds, $X_0^{U\pm}$ and $X_0^{S\pm}$, in the following way. Let X_0^P be the state vector on the periodic orbit previously obtained. Then, the initial condition for the trajectory belonging to the unstable or stable manifold will consist on adding a small perturbation ϵ to that state vector in the direction of the unstable or stable eigenvector, respectively, as in Equations (5.8) and (5.9). For clarity, Figure 5.1.4 illustrates this explanation.

$$X_0^{U\pm} = X_0^P \pm \epsilon V^U(X_0^P) \quad (5.8)$$

$$X_0^{S\pm} = X_0^P \pm \epsilon V^S(X_0^P) \quad (5.9)$$

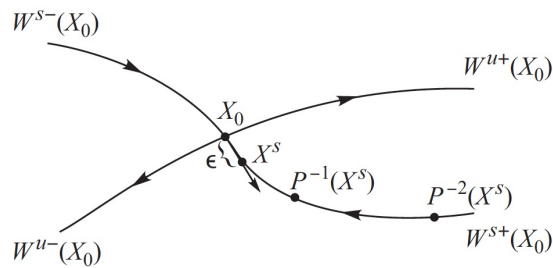


Figure 5.1.4: A simple way to compute an approximation of the two branches of the unstable ($W^{U\pm}$) or stable ($W^{S\pm}$) manifolds of a periodic orbit [28].

Figures 5.1.5a and 5.1.5b depict the unstable and stable manifolds obtained for both systems considered after integrating in the PCR3BP using initial conditions X_0^U and X_0^S . They will serve as the basis for the trajectory design detailed in the following sections. Note that due to the nature of the manifolds, starting in the periodic orbit around L_2 , we need to integrate *backwards* in time to obtain the stable manifolds depicted in the Figures, while we need to integrate *forwards* in time to obtain the unstable manifolds.

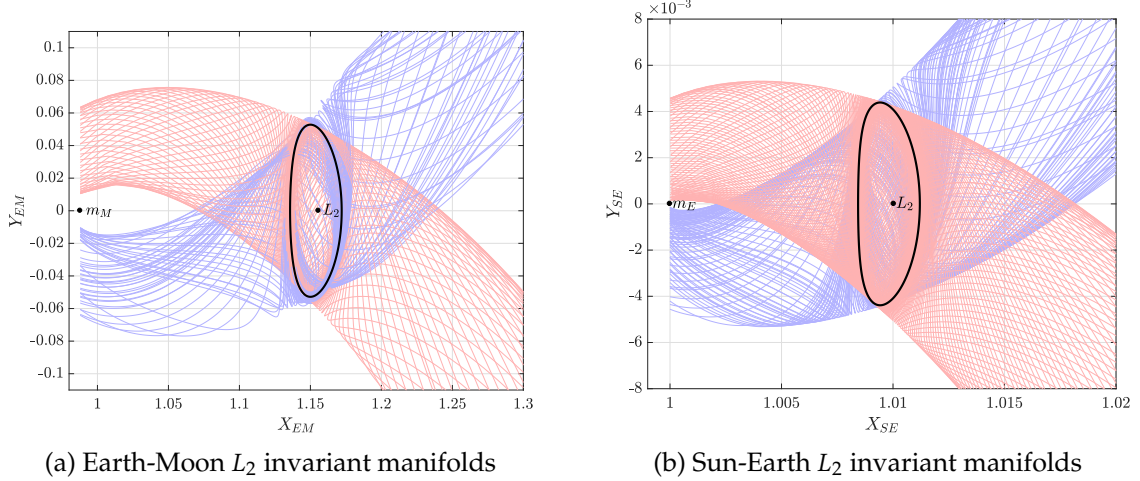
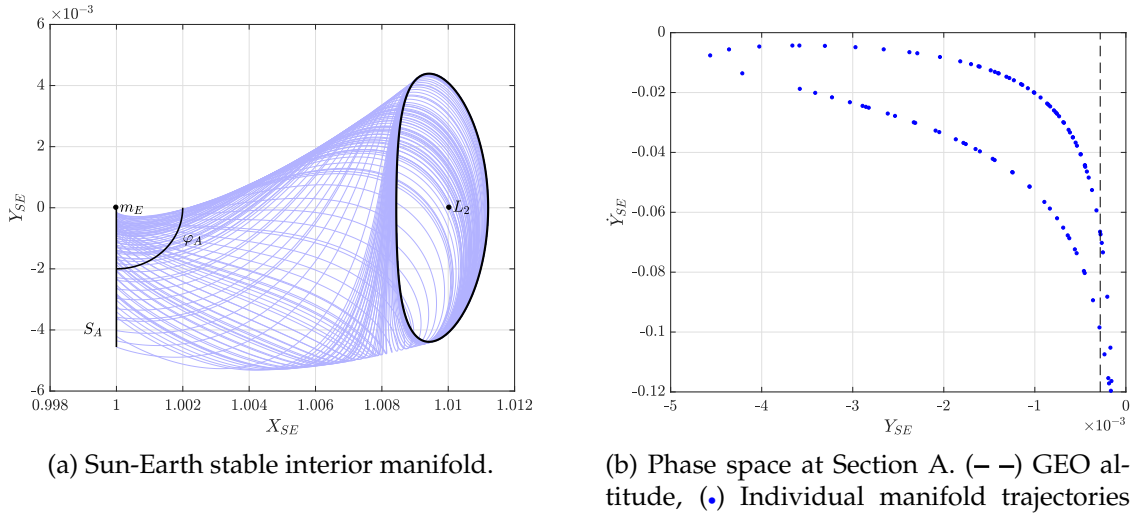


Figure 5.1.5: (—) Stable manifolds, (—) Unstable manifolds

5.1.2 Earth escape leg

Once the manifolds have been computed, the transfer trajectory will be constructed based on the state space of those manifolds on certain sections. Particularly, for the Earth escape leg, we need to choose the location of two sections, that will be defined through the angles φ_A and φ_B :

- Section A (S_A) is located such that it forms an angle φ_A in the clockwise direction with the Sun-Earth axis. Figure 5.1.6 depicts the stable interior manifold for $\varphi_A = 90^\circ$ and the corresponding state space in S_A .

Figure 5.1.6: Manifold and phase space at S_A for $\varphi_A = 90^\circ$

- Section B (S_B) is located such that it forms an angle φ_B with the Sun-Earth axis in

the counterclockwise direction. Figure 5.1.7 depicts the stable interior manifold for $\varphi_B = 90^\circ$ and the corresponding state space in S_B . Note that in our desired trajectory, the Sun-Earth and Moon-Earth trajectories will be patched precisely at S_B .

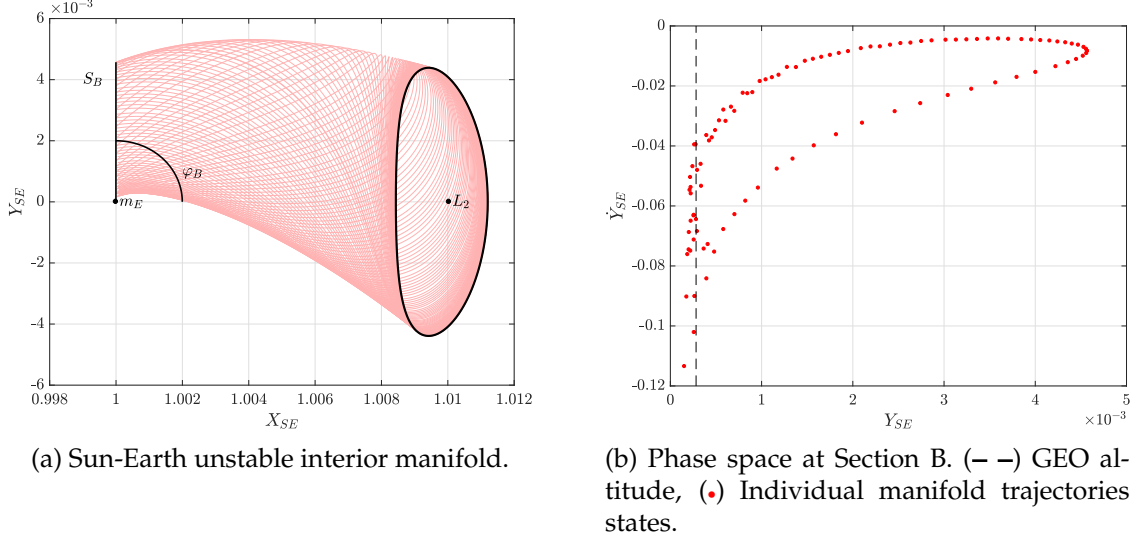


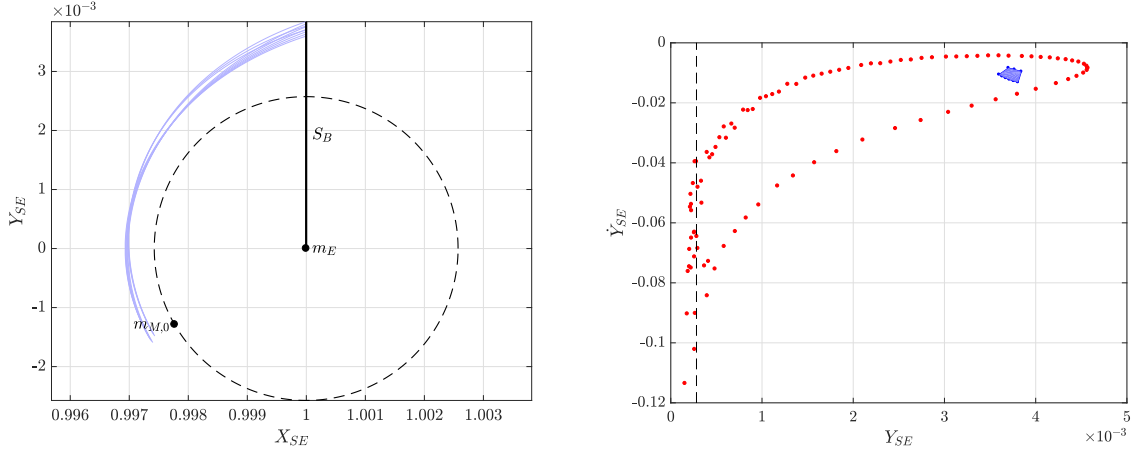
Figure 5.1.7: Manifold and phase state at S_B for $\varphi_B = 90^\circ$

5.1.3 Moon capture leg

Concerning the Moon capture leg, we will need to obtain the phase space at S_B of the Earth-Moon stable exterior manifold. For that, we need to integrate the manifolds trajectories in the Earth-Moon system backwards in time, starting at the Earth-Moon L_2 periodic orbit and until they meet S_B in the Sun-Earth system. For this, we need to know the initial angle formed by the X-axis of the Sun-Earth and the Earth-Moon systems at time t_0 , φ_0 . The value of this angle is needed to perform the change of coordinates between both systems, as explained in Section 4.1.3.

Figures 5.1.8a and 5.1.9a show the results for two values of φ_0 , namely $\varphi_0 = 210^\circ$ and $\varphi_0 = 225^\circ$. In these figures, $\varphi_B = 90^\circ$ and the Earth-Moon stable exterior manifolds are depicted after being translated into the Sun-Earth reference system. For reference, the Moon's orbit, and the position of the Moon at the beginning of the integration are also shown.

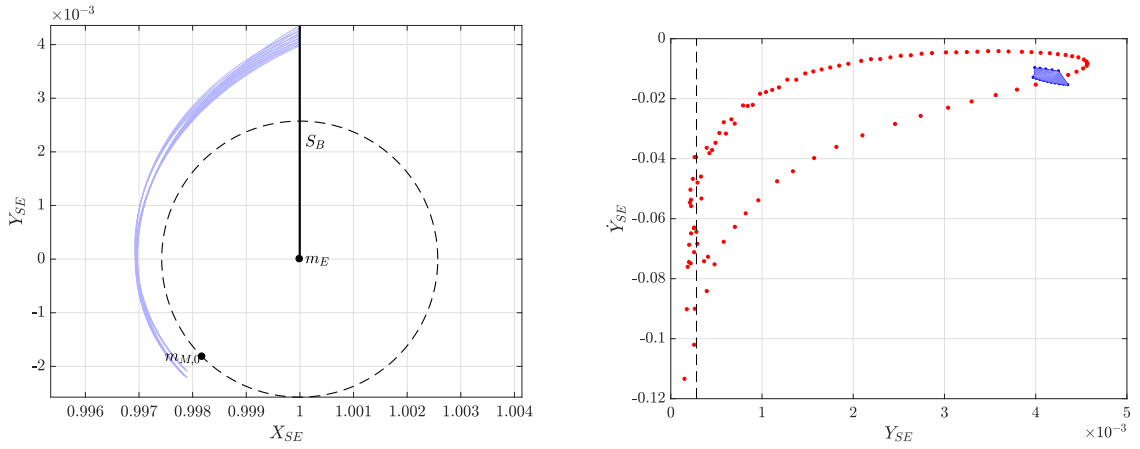
Then, Figures 5.1.8b and 5.1.9b depict the phase space on S_B of the manifolds presented in Figures 5.1.8a and 5.1.9a superposed on the phase space presented in Figure 5.1.7. Note that any point interior to the shaded blue area will approach the Earth-Moon L_2 when integrated *forward* in time. On the other hand, any point inside the area delimited by the red dots will approach the Sun-Earth L_2 when integrated *backwards* in time.



(a) Exterior stable Earth-Moon manifold. m_E and $m_{M,0}$ refer to the positions of the Earth, and the Moon at the start of the integration in the Sun-Earth system. (—) Moon orbit, (—) Manifold trajectories.

(b) Phase space at S_B . (—) GEO altitude, (●) Stable exterior Earth-Moon L_2 manifold, (●) Unstable interior Sun-Earth L_2 manifold.

Figure 5.1.8: Manifold trajectories and phase space at Section B for $\varphi_0 = 210^\circ$.



(a) Exterior stable Earth-Moon manifold. m_E and $m_{M,0}$ refer to the positions of the Earth, and the Moon at the start of the integration in the Sun-Earth system. (—) Moon orbit, (—) Manifold trajectories.

(b) Phase space at S_B . (—) GEO altitude, (●) Stable exterior Earth-Moon L_2 manifold, (●) Unstable interior Sun-Earth L_2 manifold.

Figure 5.1.9: Manifold trajectories and phase space at Section B for $\varphi_0 = 225^\circ$.

Of course, we are interested in choosing values for φ_0 and φ_B such that there is an intersection in the phase spaces coming from the Earth escape and Moon capture legs. The rationale behind this will become evident in the next section but roughly speaking, this intersection allows us to choose a patching point that will satisfy continuity, at least in x , y and \dot{y} states.

5.1.4 Trajectory patching

At this point, we need to find a way to select the two aforementioned trajectory legs so that a complete Earth-Moon coherent trajectory is obtained.

For that purpose, we will need to look back again at Figure 5.1.9b. In there, we can identify three different areas which serve to delimit states that will behave differently if used as initial state and integrated in time in the PCR3BP:

- In the region delimited by the Sun-Earth L_2 manifold states (red dots), an orbit will go back to the Sun-Earth L_2 libration point when integrated backwards in time.
- In the region delimited by the Earth-Moon L_2 manifold (blue dots), an orbit will be captured by the Moon when integrated forward in time.
- In the region inside the Earth-Moon L_2 manifold but slightly outside the Sun-Earth L_2 manifold, an orbit will get ballistically captured by the Moon when integrated forwards in time; when integrated backwards, it will follow the unstable Sun-Earth L_2 manifold, twist, and then follow the stable Sun-Earth L_2 manifold towards the Earth. This behavior is called *orbit twisting* and the amount of twisting is related to the distance of the initial condition to the manifold tube. The reader is referred to [28] for further details on the mathematical basis of this behavior.

Figures 5.1.10a and 5.1.10b depict two examples of complete initial guess trajectories obtained following this procedure. Note that the solution is very sensitive to the state selected in Section B. In this way, we can obtain trajectories like the one in 5.1.10a, in which the *orbit twisting* is very subtle and the final radius at the Earth is too large (92061 km in the example on Figure 5.1.10a). On the other hand, just changing slightly the state in Section B, we can obtain trajectories with a much more evident *orbit twisting*, which lead to a final point much closer to the Earth (28454 km in the example on Figure 5.1.10b).

The initial guess chosen to be further optimized in Chapter 6 is depicted in Figure 5.1.11. In this initial guess, $\varphi_A = 90^\circ$, $\varphi_B = 90^\circ$, $\varphi_0 = 225^\circ$, the time of transfer is 155 days and the initial altitude with respect to the Earth corresponds to a GEO orbit.

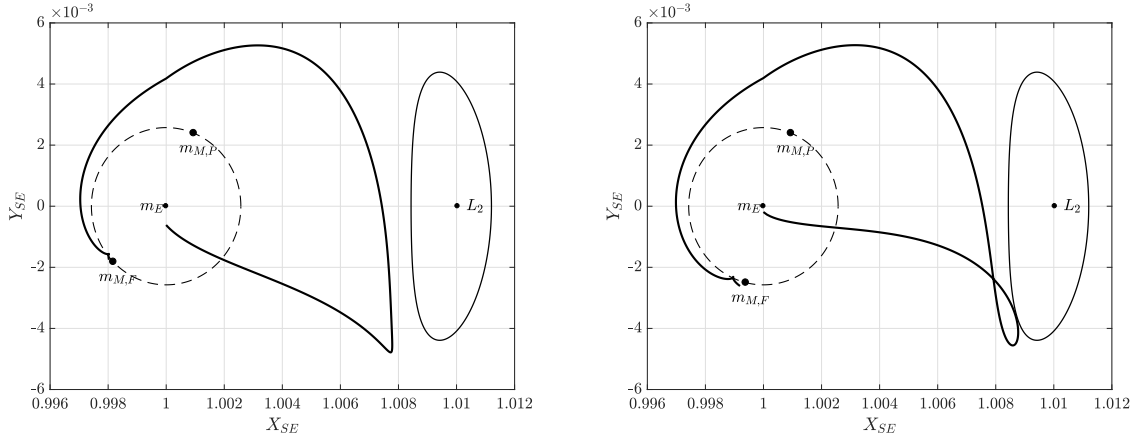


Figure 5.1.10: Examples of complete initial guess trajectories. $m_{M,F}$ and $m_{M,P}$ refer to the Moon mass position at the end of the trajectory and at the patching instant between the Earth escape and Moon capture legs; the Moon's orbit corresponds to the dashed line (—); m_E refers to the Earth mass; L_2 refers to the Sun-Earth L_2 libration point.

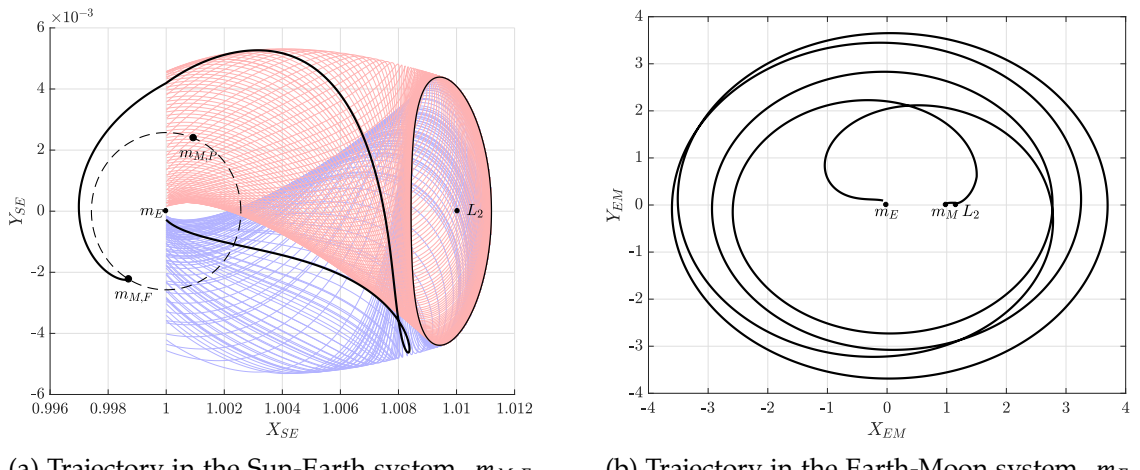


Figure 5.1.11: Complete trajectory starting from a GEO orbit, selected Initial Guess for trajectory optimization.

5.2 Initial guess based on the classical two-impulse trajectories

This section will present an alternative approach to obtain an initial guess for the Earth-Moon low-thrust transfer using the classical two-impulse strategy described in [30].

In this way, the spacecraft starting point is a parking circular orbit around the Earth. An initial burn, ΔV_0 , at the initial instant, t_0 , places it into a transfer trajectory. Then, at the final time, t_f , another impulse, ΔV_f , inserts it into a circular orbit around the Moon.

A genetic algorithm is used to span the solution space and discriminate among all possible solutions the ones that fit best. Of course, we will be interested in lowering the magnitude of the ΔV maneuver needed for the transfer. In this case, the reason behind is not only related to the size or cost of the mission, but also with its feasibility: large impulsive maneuvers cannot be provided by low-thrust systems.

5.2.1 Problem definition

First of all, it is important to note that the dynamic model used to obtain initial guesses with this approach corresponds to the PBRFBP described in Section 4.1.2, where the Earth and the Moon act as the primary bodies and the Sun acts as a perturbation.

Initially, and as it has already been discussed in Section 5.1, the spacecraft starts the Earth-Moon transfer from a circular Earth orbit of scaled radius $r_0 = (R_E + h_0)/DU$, which corresponds to a GEO parking orbit, therefore $h_0 = 35786$ km.

At the initial instant, t_0 , an impulsive maneuver ΔV_0 is executed. Of course, this maneuver needs to be performed by the launcher upper stage just prior to the Cubesat detachment. This maneuver is performed in the velocity direction, tangent to the initial circular orbit, in order to avoid complex steering maneuvers.

The goal is to choose an initial state $(x_0, y_0, \dot{x}_0, \dot{y}_0)$ and an initial and final times, (t_0, t_f) that uniquely define a solution such that the spacecraft arrives at a circular orbit around the Moon of scaled radius $r_f = (R_M + h_f)/DU$. The way chosen to identify those preferred sets of initial conditions has been the usage of a genetic algorithm to be detailed in the following section.

5.2.2 Genetic algorithm optimization

Genetic algorithms are numerical optimization algorithms inspired by both natural selection and natural genetics [54]. They are iterative methods in which the collection of possible solutions on each iteration is referred to as the *population of chromosomes*, and the transition to a new population is performed by using a sort of *natural selection* and genetics-inspired operators.

In this work, the genetic algorithm used was NSGA-II (Non-dominated Sorting Genetic Algorithm) available in [Mathworks' Matlab Central File Exchange](#).

In order to use NSGA-II, the search space of possible solutions needed to be expressed so that each population member was defined in terms of a chromosome. In the previous section, it was stated that each Earth-Moon transfer solution can be uniquely defined through the following six scalars: $(x_0, y_0, \dot{x}_0, \dot{y}_0, t_0, t_f)$. This could then constitute the six-gene chromosome of each population member. However, in order to reduce the dimensionality of the search space and therefore minimize the genetic algorithm computational time, the approach described in [30] is implemented here. In this way, the search space dimensionality is reduced from six to four by expressing the six chromosome elements as a function of only just four scalars, which are the following: $(\alpha, \beta, t_0, \delta)$, coherently with Figure 5.2.1.

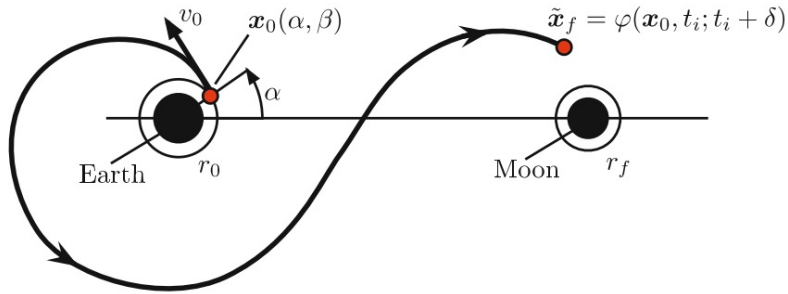


Figure 5.2.1: Direct shooting of initial guess solutions [30].

In this way, α is the angle formed by the Earth-Moon direction and the Earth-spacecraft direction at the initial time; β is the ratio of the initial spacecraft transfer velocity (just after the impulse ΔV_0) to the spacecraft velocity in the Earth circular parking orbit (just before ΔV_0); t_0 is the initial time; and δ is the transfer time. Equations 5.10 relate the six-gene initial chromosome to this newly defined four-gene chromosome, where $v_0 = \beta \sqrt{\frac{1-\mu}{r_0}}$. These four scalars become as well the *decision variables* for the genetic algorithm.

$$\begin{aligned} x_0 &= r_0 \cos \alpha - \mu \\ y_0 &= r_0 \sin \alpha \\ \dot{x}_0 &= -(v_0 - r_0) \sin \alpha \\ \dot{y}_0 &= (v_0 - r_0) \cos \alpha \end{aligned} \tag{5.10}$$

For each population member of the solution search space, the final state is found by integrating the PBRFBP starting with the initial conditions $(x_0, y_0, \dot{x}_0, \dot{y}_0; t_0)$ up to $t_f = t_0 + \delta$.

In order to select the most suitable solutions and evolve the population, NSGA-II needs to assess the fitness of the solutions against certain conditions that are given in terms of what are called *objective functions*. NSGA-II supports multi-objective optimization, meaning that we can select more than one criteria to evaluate the possible solutions. NSGA-II then sorts and evolves the population in terms of non-domination [55]. An individual is said to dominate another if the objective functions of it are no worse than the other and at least one is better. NSGA-II understands that a population member is *better* than other if their objective function evaluates to a smaller value, meaning that we need to express those

objective functions in a way that its minimization will lead to what we would consider a *better* solution.

In this work, two objective functions were used simultaneously and they correspond to Equation (5.11) and (5.12). These functions represent the error between the final state radius and the final desired Moon orbit radius, and the error between the final state velocity with respect to the Moon compared to the desired final circular velocity, V_C .

$$J_1 = \sqrt{(x_f + \mu - 1)^2 + y_f^2} - r_f \quad (5.11)$$

$$J_2 = \sqrt{(-V_C \sin \phi - (\dot{x}_f - y_f))^2 + (V_C \cos \phi - (\dot{y}_f + x_f + \mu - 1))^2} \quad (5.12)$$

where $V_C = \sqrt{\mu/r_f}$ and $\phi = \tan^{-1}(y_f/(x_f + \mu - 1))$.

In particular, the initial and final orbits were chosen to have the following altitudes: $h_0 = 35786$ km and $h_f = 1000$ km. Using GEO as a starting point for a lunar transfer makes sense since it is a standard target orbit for many spacecraft which can act as the primary payload which the Cubesat accompanies, as explained in Section 5.1. On the other hand, the altitude of the final orbit around the Moon is of the same order as the target orbits used typically for Earth-Moon low-thrust transfers in the literature [56, 57] and it is a suitable orbit to place communication relay lunar Cubesats, perform lunar exploration, etc.

Finally, another input requested by the genetic algorithm is the possible ranges for the decision variables, which in this case were:

$$\begin{aligned} \alpha &\in [0, 2\pi] \\ \beta &\in [1, \sqrt{2}] \\ t_0 &\in [0, 2\pi/\omega_s] \\ \delta &\in [1, 30] \end{aligned} \quad (5.13)$$

These limits size the four-dimensional space of possible solutions, therefore we are interesting in constraining them in order to reduce the search space and therefore the computational time; however, we do not want to be so restrictive that we might miss meaningful solutions. Concerning α , the range is straightforward: we want to explore the possibility of starting anywhere in the parking orbit; the ranges for β constrain the initial velocity (just after ΔV_0) to be in between the initial circular GEO velocity ($\beta = 1$) and the Earth-escape velocity ($\beta = \sqrt{2}$); concerning t_0 , the range chosen spans any possible configuration of the Sun, Earth, Moon system; finally, δ restricts the transfer duration to be within 4 to 130 days, which is consistent with the two-impulse Earth-Moon transfers reported in the literature.

For the optimization, a total of 500 population members and 160 generations were used. As a first step, the population is initialized. This consists on taking each population member's chromosome, evaluate the objective functions for each of them and then, sort them based on non-domination into each front. Each possible solution is assigned two attributes, which are the rank (fitness) and the crowding distance. The rank is basically the number of the front they belong to, and the crowding distance is a measure of how close an individual

is to its neighbors, serving as a measure of the population diversity [55]. The number of generations establishes the number of iterations to be performed after population initialization.

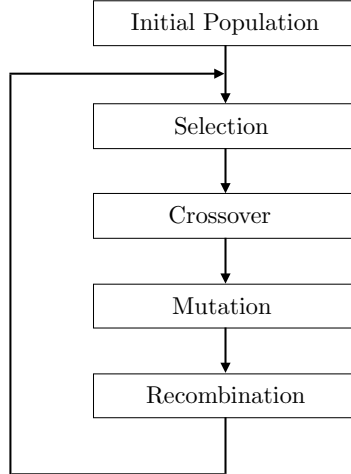


Figure 5.2.2: Sketch of the genetic algorithm process.

At each iteration, the individuals are sorted and selected using binary tournament selection. Then, the selected individuals generate offsprings through the usage of genetic operators like crossover and mutation and the process starts again. The algorithm flowchart is depicted in Figure 5.2.2. In general terms, crossover consists on taking two parent solutions and obtaining new solutions by combining them, while mutation is used to maintain the genetic diversity of the population and it consists in altering one or more genes in a chromosome from its initial state. A graphical example of both processes is depicted in Figure 5.2.3.

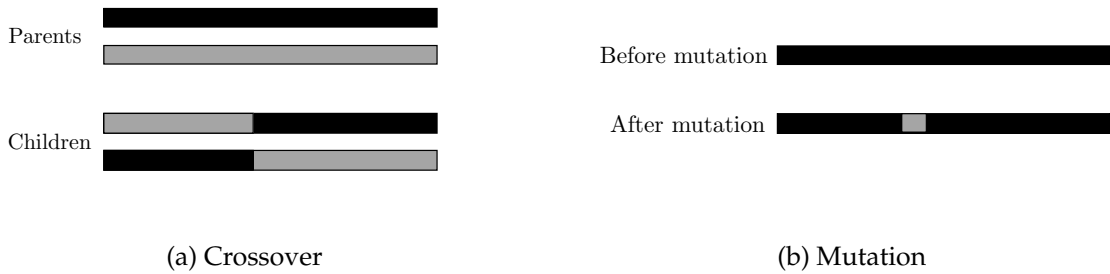
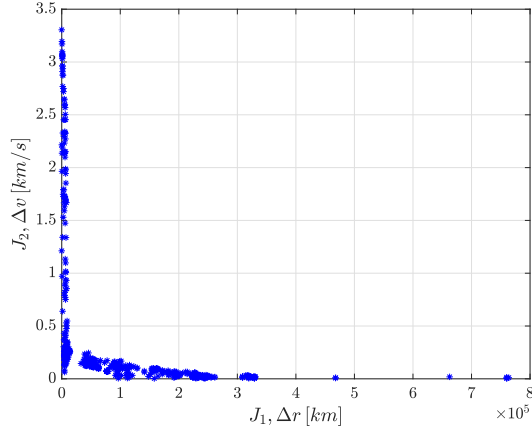


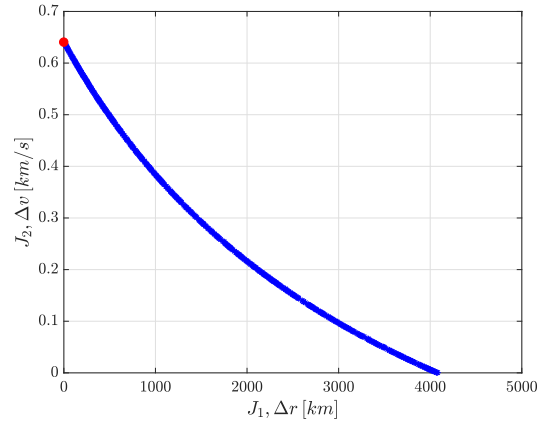
Figure 5.2.3: Example of the genetic algorithm operators.

The Pareto front obtained after optimization is depicted in Figure 5.2.4. On the other hand, the population is mapped in terms of one of the objective functions and the time of transfer in Figures 5.2.5 and 5.2.6. As it can be seen, after 160 generation the population is quite homogeneous in terms of δ . Additionally, the selected solution chosen as initial guess is depicted in the Pareto fronts with a red dot. The rationale behind this choice was the following: to select the solution with minimum Δr whose associated Δv is small enough so that it can be translated into a series of low thrust burns in the optimization procedure.

In other words, we selected a solution with minimum Δr (implying a larger Δv) and used it as input for the optimization procedure described in Chapter 6. In the end, we were able to converge to an acceptable solution and therefore the iteration process on the initial guess need not to continue. If, on the other hand, no feasible solution was obtained in the optimization process, another initial guess with a lower Δv should have been selected at a cost of arriving at a point at a larger Δr from our original target.

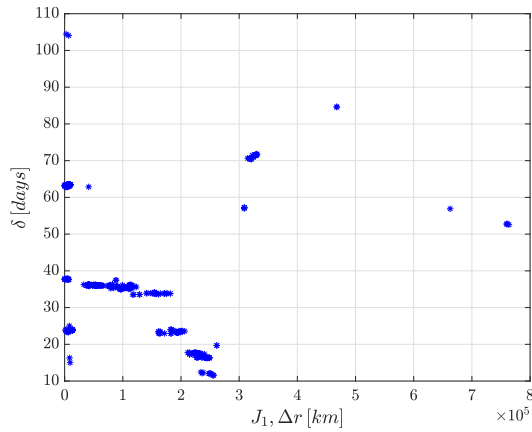


(a) Results after 20 generations

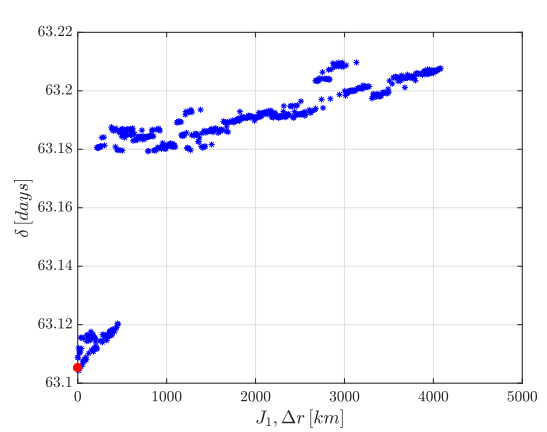


(b) Results after 160 generations

Figure 5.2.4: Pareto front obtained from the genetic algorithm implementation in terms of the two specified objective functions, (●) Selected initial guess.



(a) Results after 20 generations



(b) Results after 160 generations

Figure 5.2.5: Population of chromosomes in terms of one of the objective functions, J_1 , and the time of transfer, δ . (●) Selected initial guess.

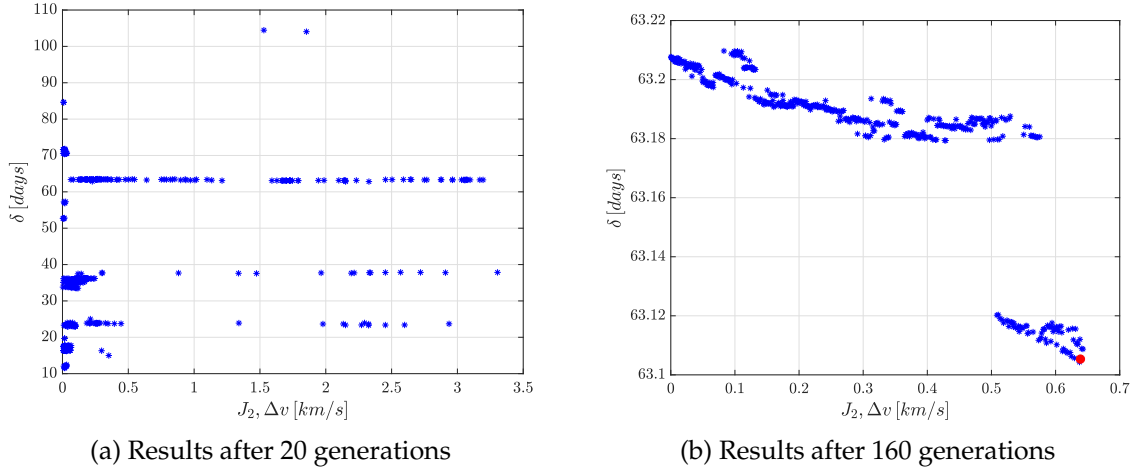


Figure 5.2.6: Population of chromosomes in terms of one of the objective functions, J_2 , and the time of transfer, δ . (●) Selected initial guess.

Integrating in the PBR4BP the selected solution, the trajectory obtained was the one depicted in Figure 5.2.7. The details on this initial guess are described below:

$$\begin{aligned} \alpha &= 308.03^\circ, \quad \beta = 1.3449 \rightarrow \Delta V_0 = 1.06 \text{ km/s}, \quad t_0 = 0, \\ \delta &= 63 \text{ days}, \quad \Delta V_f = 0.639 \text{ km/s}, \quad \Delta r = 4.39 \text{ km} \end{aligned} \quad (5.14)$$

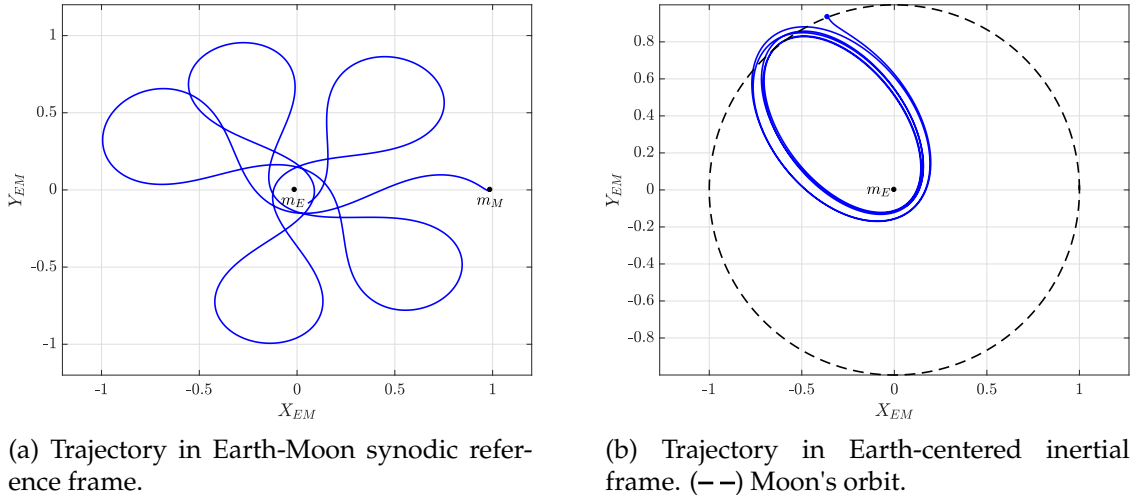


Figure 5.2.7: Selected initial guess for the Earth-Moon transfer.

Chapter 6

Optimization Problem

The methods presented in Chapter 5 and used to construct initial guesses for the Earth-Moon transfers were defined in the literature and have mostly been used for *impulsive transfers*. It is, they are built on the underlying assumption that the spacecraft propulsion system will be able to execute a ΔV maneuver in a time that is ideally, infinitely small. However, the micropropulsion systems compatible with Cubesats (see Section 2.2) lack those capabilities. Therefore, we need to define the appropriate thrust evolution so that the spacecraft is able to perform the Earth-Moon transfer in a way that it is feasible not only from an Astrodynamics point of view but also from a systems engineering point of view.

For that, the trajectory will be optimized using a Non-Linear Programming method. A general description of the solver's methodology and the problem definition will be presented below.

6.1 Optimal Control

Optimal control is a subject whose goal is to determine the inputs to a dynamical system to optimize (i.e., minimize or maximize) a specified performance criterion while satisfying any constraints on the motion of the system. Because of the complexity of most applications, optimal control problems are most often solved numerically [58].

The general optimal control problem statement is as follows (extracted from [58]): determine the *state*, $x(t) \in \mathbb{R}^n$, the control, $u(t) \in \mathbb{R}^m$, the vector of static parameters, $p \in \mathbb{R}^q$, the initial time, $t_0 \in \mathbb{R}$, and the terminal time, $t_f \in \mathbb{R}$, that optimize the performance index J in Equation (6.1).

$$J = \Phi[x(t_0), t_0, x(t_f), t_f; p] + \int_{t_0}^{t_f} \mathcal{L}[x(t), u(t), t; p] dt \quad (6.1)$$

The solution also has to fulfill the dynamic constraints (Equation (6.2)), the path constraints (Equation (6.3)) and the boundary conditions (Equation (6.4)).

$$\dot{x}(t) = f[x(t), u(t), t; p] \quad (6.2)$$

$$C_{\min} \leq C[x(t), u(t), t; p] \leq C_{\max} \quad (6.3)$$

$$\phi_{\min} \leq \phi[x(t_0), t_0, x(t_f), t_f; p] \leq \phi_{\max} \quad (6.4)$$

Numerical methods for solving optimal control problems can be broadly classified into direct and indirect methods. Indirect methods perform the optimization task by requiring that the first variation of the performance index must be zero at the solution. They are based on the *Calculus of Variations* [59] and the determination of the first order optimality conditions, resulting from Pontryagin's minimum principle. This leads to solving directly a multiple-point boundary-value problem to determine candidate optimal trajectories called *extremals*. Alternatively, direct methods minimize or maximize the performance index directly by making appropriate changes to the input variables [27]. For that, they discretize the state/control so that the infinite dimensional problem is translated into a finite optimization problem which is solved using Non-Linear Programming (NLP) solvers, that use complex mathematical programming techniques. For a detailed taxonomy of trajectory optimization methods, the reader is referred to [56].

Although there is a great variety of NLP methods, in a broad sense, they can be categorized into shooting methods and transcription or collocation methods. In direct shooting, only the control vector is parameterized to transcribe the infinite-dimensional optimal control problem into a finite-dimensional nonlinear program (NLP). Typically, this NLP is smooth and can be solved by gradient-based algorithms like sequential quadratic programming (SQP) or interior-point methods [60]. On the other hand, in direct collocation methods both the state and the control are approximated using piece-wise continuous polynomials and the constraints on dynamics are imposed on intermediate points (called collocation points). The optimal solution is required to satisfy the conditions of optimality at these intermediate points only.

Another important category of numerical methods for solving optimal control problems are pseudospectral methods. Pseudospectral methods can be described as a global form of orthogonal collocation in which the state is approximated using a global polynomial and collocation is performed at chosen points [58]. In a pseudospectral method, the number of meshes is fixed and the degree of the polynomial is varied, whereas in local collocation, the degree of the polynomial is fixed and the number of meshes is varied.

In this work, the Gauss Pseudospectral Optimization Software (GPOPS) has been used to solve the optimal control problem. GPOPS is a software program written in MATLAB capable of solving multi-phase optimal control problems [61]. In this case, the GPOPS software was used in conjunction with a direct collocation method and the solver IPOPT (Interior Point Optimizer).

Concerning the direct transcription or collocation method, Hermite-Simpson approach, illustrated in Figure 6.1.1, was used. In this way, time is discretized and for each of the segments $[t_k, t_{k+1}]$, the two end points, denoted as *nodes*, represent the corresponding state and

control NLP variables $[x_k, u_k, x_{k+1}, u_{k+1}]$. The dynamics are used to provide time derivative values at the two nodes, so the four pieces of information $[x_k, x_{k+1}, f(x_k, u_k), f(x_{k+1}, u_{k+1})]$ can be used to construct a third-order Hermite interpolate polynomial. Note that in this way, the interpolate polynomial can only satisfy the dynamics at the nodes.

However, this method also enforces the equations of motion at a third point, which is located at t_c , the middle point of $[t_k, t_{k+1}]$, and is called *collocation point*. This is done by enforcing $\nabla = \dot{x}_c = f(x_c, u_c) = 0$, where $[x_c, u_c]$ are the state and control at t_c . In this way, the polynomial satisfies the dynamics at the nodes and the collocation points. If a large number of intervals are used, the state motion approaches the real dynamics within the whole time domain [62].

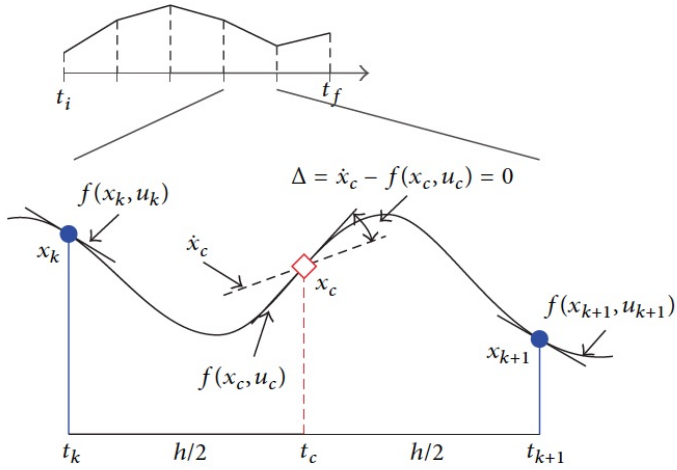


Figure 6.1.1: Hermite-Simpson collocation method (third-degree interpolant) [62].

Once the problem is transcribed into a finite NLP problem, IPOPT solver is used. IPOPT is an open source software package for large-scale nonlinear optimization. It can be used to solve general nonlinear programming problems of the form

$$\begin{aligned} & \min_{x \in \mathbb{R}^n} f(x) \\ \text{such that } & g^L \leq g(x) \leq g^U \\ & x^L \leq x \leq x^U \end{aligned} \tag{6.5}$$

where $x \in \mathbb{R}^n$ are the optimization variables and the superindexes L and U refer to the lower and upper bounds, respectively ($x^L \in (\mathbb{R} \cup \{-\infty\})^n$, $x^U \in (\mathbb{R} \cup \{+\infty\})^n$), $f : \mathbb{R}^n \rightarrow \mathbb{R}$ is the objective function, and $g : \mathbb{R}^n \rightarrow \mathbb{R}^m$ are the general nonlinear constraints. The functions $f(x)$ and $g(x)$ can be linear or nonlinear and convex or non-convex (but should be twice continuously differentiable). The constraints, $g(x)$, have lower and upper bounds, $g^L \in (\mathbb{R} \cup \{-\infty\})^m$, $g^U \in (\mathbb{R} \cup \{+\infty\})^m$. IPOPT implements an interior point search filter method that aims to find a local solution of (6.5) [63]. More information on the mathematical details of the algorithm can be found in [64].

6.2 Problem definition

The goal of the optimization process is to obtain the thrust magnitude and direction that will allow the spacecraft to perform the Earth-Moon transfer with the lowest fuel consumption consistently with the PBRFBP dynamics and the appropriate constraints.

In this way, the dynamics of the optimization problem are the ones in Equations (6.6) to (6.8). Note that these equations of motion are identical to the ones presented in Section 4.1.2 except for the fact that we have added the acceleration coming from the spacecraft thrust. Therefore, the four-body potential Ω_4 is the same as the one defined in Equation (4.14). Besides, we needed to add the equation describing the evolution of the spacecraft mass, m , for full consistency.

$$\ddot{x} = \frac{\partial \Omega_4}{\partial x} + 2\dot{y} + \frac{\tau T_{max} \cos \theta}{m} \quad (6.6)$$

$$\ddot{y} = \frac{\partial \Omega_4}{\partial y} - 2\dot{x} + \frac{\tau T_{max} \sin \theta}{m} \quad (6.7)$$

$$\dot{m} = -\frac{\tau T_{max}}{I_{sp}g_0} \quad (6.8)$$

In these equations, T_{max} and I_{sp} are the maximum thrust and the specific impulse of the spacecraft propulsion system, and g_0 is the standard acceleration due to gravity on the surface of the Earth. Then, the controls of the system are the following: τ , which is the throttle of the propulsion system, and θ , which is the angle made by the thrust vector with the Earth-Moon synodic reference frame x-axis.

The dimensions of this optimal control problem are the following: $x(t) \in \mathbb{R}^5$, $u(t) \in \mathbb{R}^2$, $p \in \emptyset$. In other words, the state is a vector of five components, namely, x and y position and velocity, and spacecraft mass (Equation (6.9)); and the control vector is composed by the thrust throttle and the thrust direction angle (Equation (6.10)).

$$x(t) = \begin{bmatrix} x(t) \\ y(t) \\ m(t) \\ \dot{x}(t) \\ \dot{y}(t) \end{bmatrix} \quad (6.9)$$

$$u(t) = \begin{bmatrix} \tau(t) \\ \theta(t) \end{bmatrix} \quad (6.10)$$

In this case, the goal was to minimize the fuel consumption, since the amount of fuel needed to carry onboard is a very important factor concerning the overall cubesat size and weight limitations. Therefore, the objective function to be minimized was the following:

$$J = -m_f \quad (6.11)$$

Concerning the path constraints, both the controls and the states need to be bounded, as stated in Equations (6.12), (6.13).

$$0 \leq \theta(t) \leq 2\pi, \quad 0 \leq \tau(t) \leq 1 \quad (6.12)$$

$$\begin{bmatrix} x_{min} \\ y_{min} \\ m_{min} \\ \dot{x}_{min} \\ \dot{y}_{min} \end{bmatrix} \leq \begin{bmatrix} x(t) \\ y(t) \\ m(t) \\ \dot{x}(t) \\ \dot{y}(t) \end{bmatrix} \leq \begin{bmatrix} x_{max} \\ y_{max} \\ m_{max} \\ \dot{x}_{max} \\ \dot{y}_{max} \end{bmatrix} \quad (6.13)$$

In GPOPS, boundary conditions are inserted in two different ways: on one hand, bounds for the initial and terminal states and times need to be provided (Equation (6.14), (6.15), (6.16), (6.17)); on the other hand, extra boundary conditions of the form $\phi = f(x(t_0), t_0, x(t_f), t_f; p)$ can be imposed as well and are referred to as *events*. Those constraints imposed through *events* will depend on the type of final orbit we are targeting, among others, and will be detailed in Section 7.1 for each solution presented.

$$\begin{bmatrix} x_{0,min} \\ y_{0,min} \\ m_{0,min} \\ \dot{x}_{0,min} \\ \dot{y}_{0,min} \end{bmatrix} \leq \begin{bmatrix} x_0 \\ y_0 \\ m_0 \\ \dot{x}_0 \\ \dot{y}_0 \end{bmatrix} \leq \begin{bmatrix} x_{0,max} \\ y_{0,max} \\ m_{0,max} \\ \dot{x}_{0,max} \\ \dot{y}_{0,max} \end{bmatrix} \quad (6.14)$$

$$\begin{bmatrix} x_{f,min} \\ y_{f,min} \\ m_{f,min} \\ \dot{x}_{f,min} \\ \dot{y}_{f,min} \end{bmatrix} \leq \begin{bmatrix} x_f \\ y_f \\ m_f \\ \dot{x}_f \\ \dot{y}_f \end{bmatrix} \leq \begin{bmatrix} x_{f,max} \\ y_{f,max} \\ m_{f,max} \\ \dot{x}_{f,max} \\ \dot{y}_{f,max} \end{bmatrix} \quad (6.15)$$

$$t_{0,min} \leq t_0 \leq t_{0,max} \quad (6.16)$$

$$t_{f,min} \leq t_f \leq t_{f,max} \quad (6.17)$$

Chapter 7

Results and Discussion

At this point, the general procedure to obtain Earth-Moon transfer trajectories has been explained in detail, including both the initial guess construction and the optimization problem. Indeed, the potential of this work lies precisely on its generality, since it is formulated in a way that can be easily customized for the requirements of any given lunar mission. In this chapter, four different solutions will be presented. Particularly, we will compare the type of trajectories found with the two different initial guesses selected and we will discuss the resulting trajectories in terms of feasibility, comparison with values reported in the literature, and possible lunar missions that could benefit from these kinds of trajectories.

7.1 Optimization results

Although the procedures and problem definition have been formulated generally and are valid for any given cubesat system, in order to provide concrete results, a cubesat with the following characteristics has been considered, corresponding to state of the art values on micropulsion (see Section 2.2) and a 2 U cubesat:

- $I_{sp} = 2000$ s
- $T_{max} = 300 \mu\text{N}$
- $m_0 = 2 \text{ kg}$

In this section, four different example trajectories will be presented. Those trajectories have been obtained from solving the optimal control problem described in Chapter 6. Note that the solutions provided as initial guesses to GPOPS for the position and velocity states are the ones obtained as output in Chapter 5, depicted in Figures 5.1.11 and 5.2.7. Concerning the initial guess for the mass evolution, the approach was to use $m(t) = m_0$; for the controls, $\tau(t) = \theta(t) = 0$ was stated as initial guess.

The following subsections will detail the path constraints used in order to retrieve each of the presented optimized trajectories as well as the associated states and control evolution obtained.

7.1.1 Trajectory A

This trajectory has been obtained starting from the initial guess computed with the classical two-impulse method, that is, the one presented in Figure 5.2.7. The final target orbit has been chosen to correspond to a circular orbit around the Moon.

Concerning the optimal control problem implementation and imposed bounds, since the initial state in the GEO orbit is in fact the result of the NSGA-II optimization, we constrained the optimized trajectory initial position and velocity to be the same as the ones obtained from the initial guess. Note that a 1% margin was used for the velocity in the synodic reference frame in order to facilitate the obtention of a feasible solution. The rationale behind this is that, since the burn will be provided by an external device, we have some flexibility on its magnitude. However, we do not have that flexibility concerning the burn direction; it needs to be parallel to the GEO velocity in order to avoid complex steering maneuvers. This is enforced with the path constraint in Equation (7.1). Note that a small tolerance $\epsilon = 10^{-20}$ has been used when using this type of constraints in order to avoid convergence issues coming from the fact that there is a finite numerical accuracy associated with the computations.

$$|(x_0 + \mu)(\dot{x}_0 - y_0) + y_0(\dot{y}_0 + x_0 + \mu)| \leq \epsilon \quad (7.1)$$

Then, the final state has to be such that its position and velocity leave the spacecraft in a circular orbit around the Moon. This was imposed mathematically as follows:

$$\sqrt{((\dot{x}_f - y_f) + V_c \sin \gamma)^2 + ((\dot{y}_f + x_f + \mu - 1) - V_c \cos \gamma)^2} \leq \epsilon \quad (7.2)$$

where $r_f = \sqrt{(x_f - 1 + \mu)^2 + y_f^2}$ is the distance to the Moon, $V_c = \sqrt{\mu/r_f}$ is the velocity for a lunar circular orbit of radius r_f and $\gamma = \tan^{-1}(y_f/(x_f - 1 + \mu))$ is the angle formed by the line joining the Moon-spacecraft direction and the Earth-Moon x-axis. In other words, Equation (7.2) is the vectorial difference of the final spacecraft velocity in the non-synodic frame and the velocity corresponding to a circular orbit of radius r_f .

Figure 7.1.1 gathers the results obtained from the optimization. Figure 7.1.1a compares the initial guess and the optimized trajectory, and as it can be seen, although there are some differences, the overall behavior is maintained and the two trajectories are quite similar geometrically.

Figure 7.1.1b depicts the results of integrating the final states coming from the optimized trajectory in the PBRFBP dynamics without thrust; this serves as a confirmation that indeed, our trajectory leaves the spacecraft in a circular lunar orbit of altitude $h_c = 723$ km.

Figures 7.1.1c and 7.1.1d show the controls evolution. As it can be seen, thrusting is continuous along the trajectory although the throttle setting and the direction keep fluctuating. According to this, the mass fraction profile is quite smooth, with a final m_f/m_0 of 0.9895. Finally, the initial impulse required to be performed externally on the cubesat is $\Delta V_0 = 1.0508$ km/s and the transfer lasts 63.4 days.

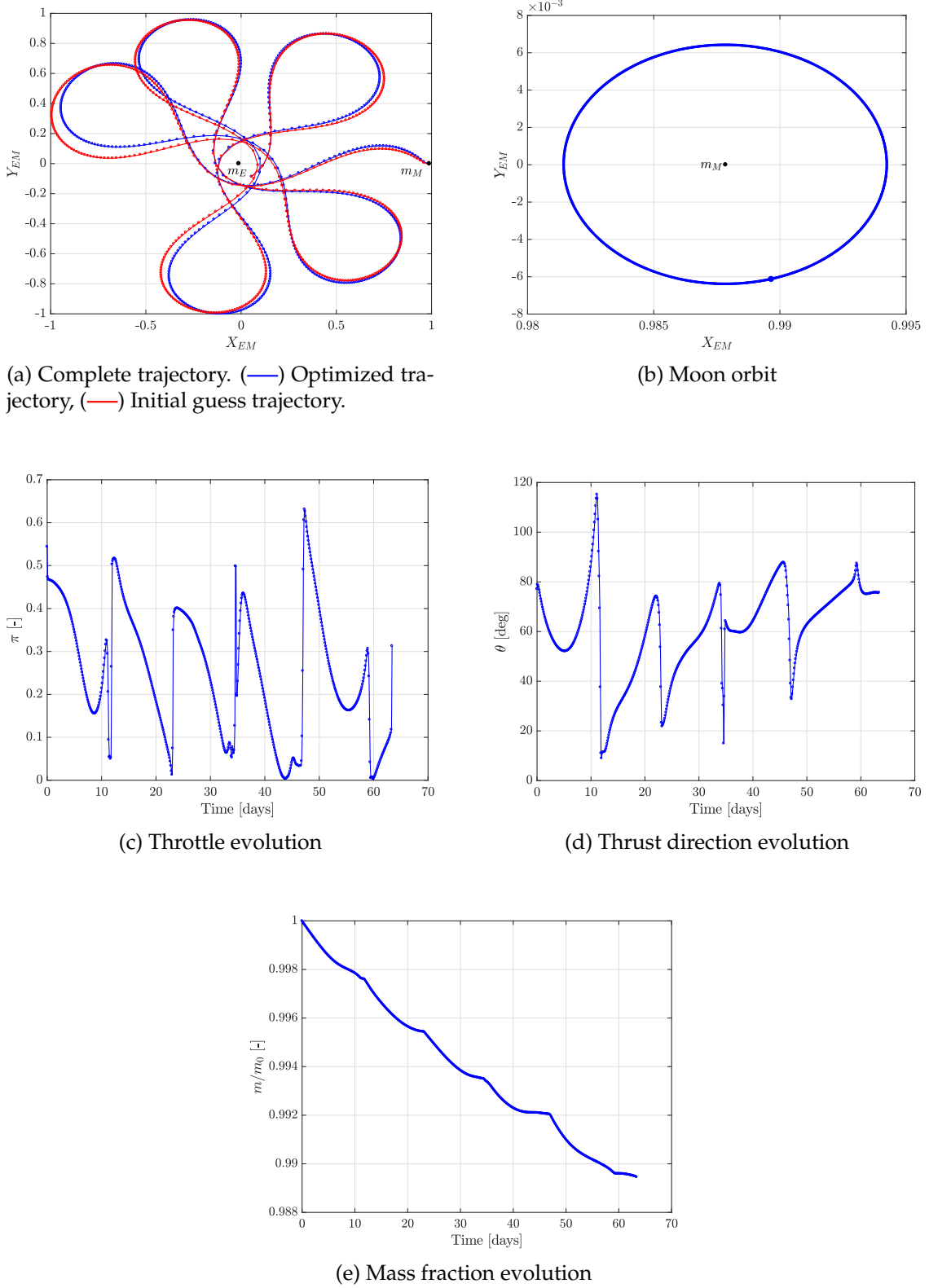


Figure 7.1.1: Trajectory A results.

7.1.2 Trajectory B

Trajectory B has also been obtained from the two-impulse initial guess and therefore, the optimal control setup is very similar to the one used for Trajectory A. In this way, the initial and terminal states and time bounds were the same. Again, Equation (7.1) was used to enforce the direction of the initial ΔV_0 .

However, the *events* constraining the final state were quite different, since in this case we were aiming at an elliptic orbit that would allow us to reach a lower altitude over the Moon during the periapsis passage.

For that, we imposed Equation (7.3) to assure perpendicularity of position and velocity vectors with respect to the Moon at the final state. This means that at this point, we are arriving at either the apoapsis or the periapsis of the final elliptic orbit. Then, we set up constraints making use of the *vis-viva equation* (Equation (7.4)), where a is the semimajor axis of the orbit. Note that the *vis-viva equation* only holds for the two body problem and we are dealing with a four body problem; however, here it is been used for constraints imposed on the final state, which is well inside the Moon's sphere of influence. Therefore, we can neglect the influence of the Sun and the Earth in this particular case, the two body problem being a good enough approximation.

$$|(x_f + \mu - 1)(\dot{x}_f - y_f) + y_f(\dot{y}_f + x_f + \mu - 1)| \leq \epsilon \quad (7.3)$$

$$\frac{-\mu}{2a} = \frac{v^2}{2} - \frac{\mu}{r} \quad (7.4)$$

In this way, at each algorithm iteration, the energy of the orbit at the final trajectory state was calculated and from it, the periapsis and apoapsis of the potential elliptical orbit were computed:

$$r_p = \min(r_f, 2a - r_f), \quad r_a = 2a - r_p \quad (7.5)$$

where a was obtained from Equation (7.4).

The final constraints used were the following:

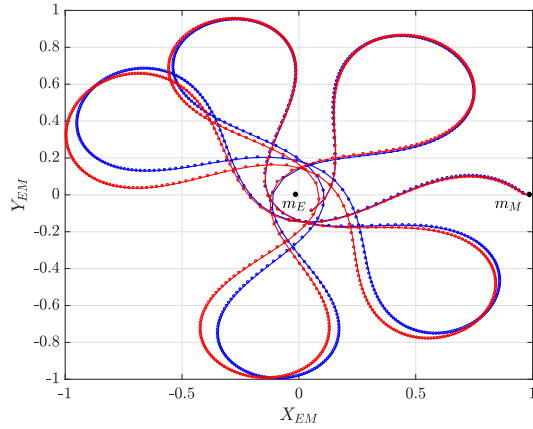
$$(100 + R_{moon}) \cdot 10^3 / DU \leq r_p \leq (500 + R_{moon}) \cdot 10^3 / DU \quad (7.6)$$

$$(500 + R_{moon}) \cdot 10^3 / DU \leq r_a \leq (5000 + R_{moon}) \cdot 10^3 / DU \quad (7.7)$$

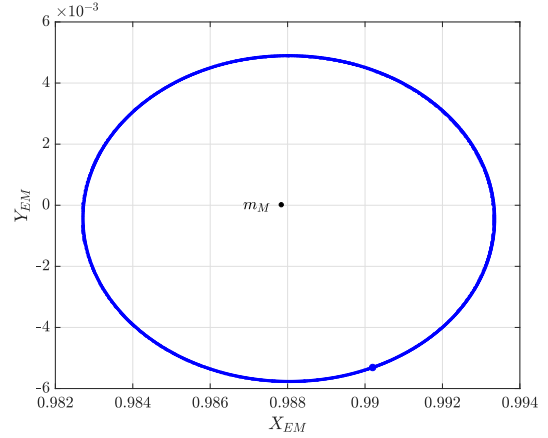
where R_{moon} corresponds to the radius of the Moon, namely, 1738 km.

Figure 7.1.2 gathers the results obtained. The optimized trajectory matches quite well the initial guess. As it can be seen in Figure 7.1.2b, the final orbit around the Moon is elliptic, with $h_p = 123$ km and $h_a = 500$ km. The total transfer time was 63.3 days and the initial impulse needed has a magnitude of $\Delta V_0 = 1.0506$ km/s. These results are pretty

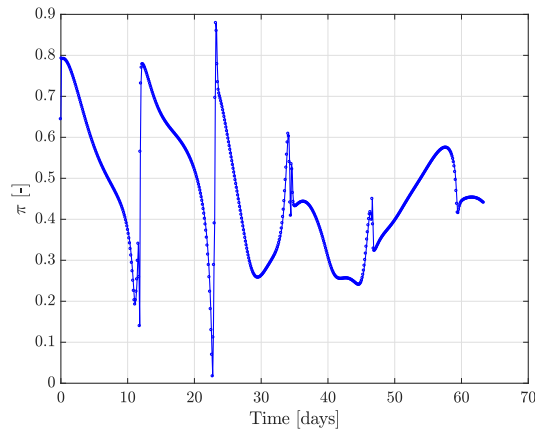
similar to the ones presented for Trajectory A, with a slightly higher mass consumption, since $m_f/m_0 = 0.9805$ in this case.



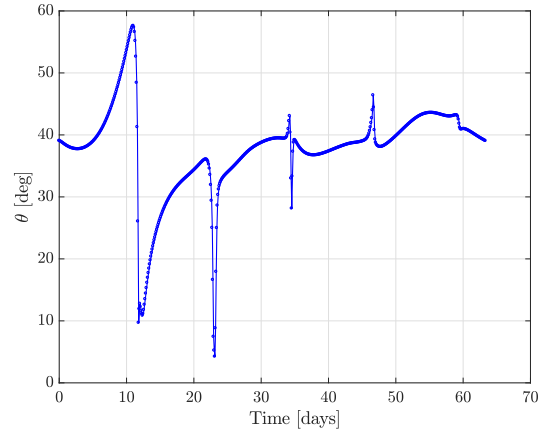
(a) Complete trajectory. (—) Optimized trajectory, (---) Initial guess trajectory.



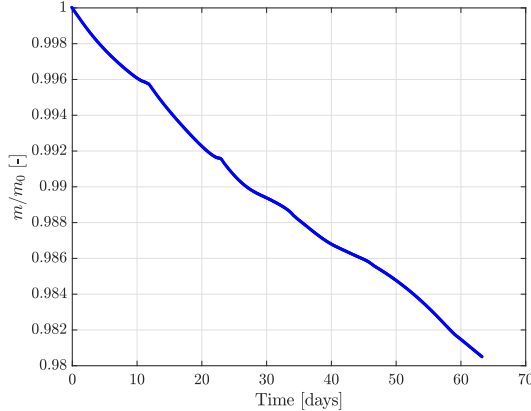
(b) Moon orbit



(c) Throttle evolution



(d) Thrust direction evolution



(e) Mass fraction evolution

Figure 7.1.2: Trajectory B results.

7.1.3 Trajectory C

As opposed to A and B, trajectory C has been obtained starting from the invariant manifolds initial guess presented in Figure 5.1.11.

In this case, the initial position and velocity were not optimized in the initial guess construction process: instead, we just looked for manifold trajectories that would cross Section S_A at a distance from the Earth corresponding to the GEO radius. Due to this fact, we will not constrain the optimized trajectory to have the same initial state as the initial guess and we will impose very flexible bounds; however, we will still constrain the initial position to be placed at GEO altitude and the initial external burn to be parallel to the velocity at that GEO orbit. This is done by bounding the initial radius with respect to the Earth (Equation (7.8)), constraining the initial position and velocity vectors with respect to the Earth to be perpendicular (Equation (7.9)) and bounding the magnitude of the initial impulse to a reasonable value (Equation (7.10)).

$$r_{GEO} - \epsilon \leq \sqrt{(x_0 + \mu)^2 + y_0^2} \leq r_{GEO} + \epsilon \quad (7.8)$$

$$(x_0 + \mu)(\dot{x}_0 - y_0) + y_0(\dot{y}_0 + x_0 + \mu) \leq \epsilon \quad (7.9)$$

$$0 \leq \sqrt{(\dot{x}_0 - y_0 + V_{GEO} \sin \gamma_0)^2 + (\dot{y}_0 + x_0 + \mu - V_{GEO} \cos \gamma_0)^2} \leq \frac{1}{2} V_{GEO} \quad (7.10)$$

$$V_{GEO} = \sqrt{\frac{1 - \mu}{r_{GEO}}}, \quad \gamma_0 = \tan^{-1}(y_0, x_0 + \mu)$$

Concerning the final state, the following constraints were imposed in order to limit the final orbit radius to have an appropriate altitude to be useful for lunar missions, and to make sure the final velocity corresponds to a circular orbit around the Moon.

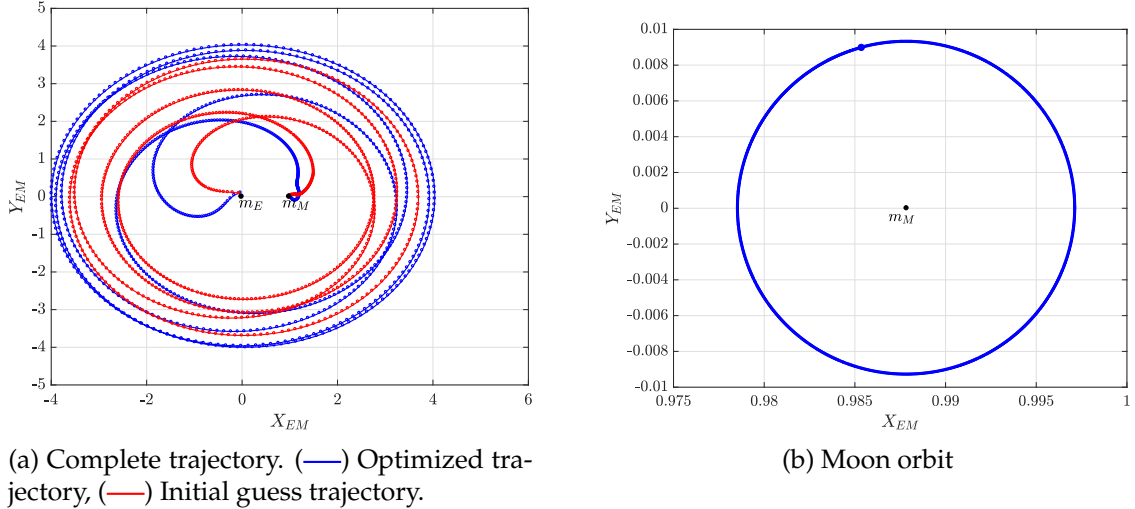
$$(100 + R_{moon}) \cdot 10^3 / DU \leq \sqrt{(x_f - 1 + \mu)^2 + y_f^2} \leq (8000 + R_{moon}) \cdot 10^3 / DU \quad (7.11)$$

$$\sqrt{((\dot{x}_f - y_f) + V_c \sin \gamma)^2 + ((\dot{y}_f + x_f + \mu - 1) - V_c \cos \gamma)^2} \leq \epsilon \quad (7.12)$$

where R_{moon} and V_c has been defined in Sections 7.1.1 and 7.1.2.

Figure 7.1.3 depicts the results obtained. As it can be seen, there is a noticeable difference between the initial guess and the optimized trajectory. This was expected, for several reasons. First of all, they have been constructed using different dynamic models, namely, two patched 3BP and 4BP, respectively. Moreover, the initial velocity of the initial guess trajectory was not parallel to the GEO velocity and that is the reason why the two trajectories are quite different during the Earth escape phase. Finally, at the patching point of the initial guess there exists a small patching impulse that it is not accounted for in the initial guess for the throttle or thrust direction, meaning that the initial guess dynamics are not fully coherent at that point.

Nonetheless, we were able to obtain a solution for a trajectory leading to a final lunar orbit of $h_c = 1835$ km, as it can be seen in Figure 7.1.3b. The throttle evolution (Figure 7.1.3c) is very different from the ones observed in the previous trajectories since it exhibits more differentiated regions of low and high throttle, with sharp transitions between them. This is clearly reflected in the mass fraction evolution (Figure 7.1.3e) with plateaus corresponding to the low throttle periods and leading to $m_f/m_0 = 0.9856$ at the end of the transfer. The impulsive burn needed at the initial instant is $\Delta V_0 = 1.2084$ km/s and the transfer time is 154.2 days.



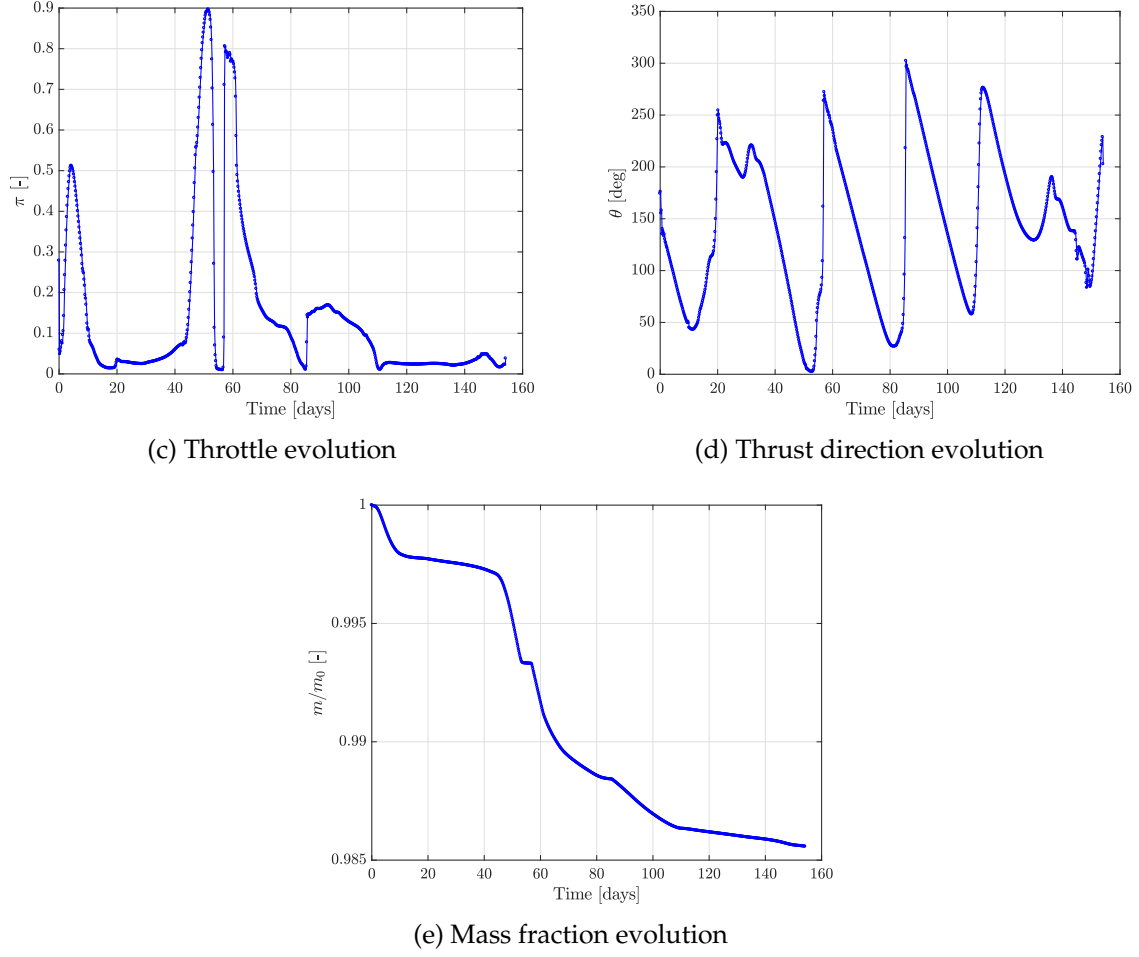


Figure 7.1.3: Trajectory C results.

7.1.4 Trajectory D

Similarly to trajectory C, trajectory D stems from the invariant manifolds initial guess, the difference being that in this case, we are targeting elliptical orbits.

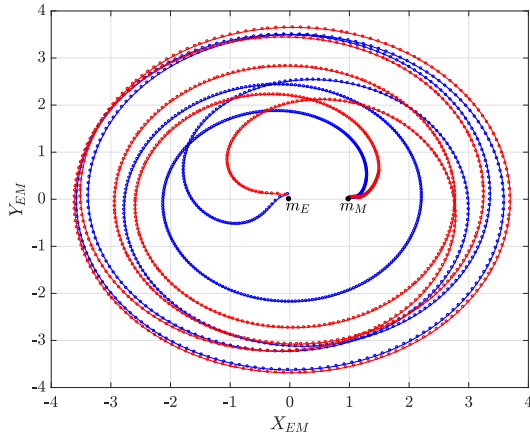
For this reason, the path constraints for the initial state are the same as those used in trajectory C; however, for the final states we used the same philosophy as in trajectory B, using the *vis-viva equation* to arrive at elliptical orbits of given periapsis and apoapsis altitudes. The final state constraints were then:

$$|(x_f + \mu - 1)(\dot{x}_f - y_f) + y_f(\dot{y}_f + x_f + \mu - 1)| \leq \epsilon \quad (7.13)$$

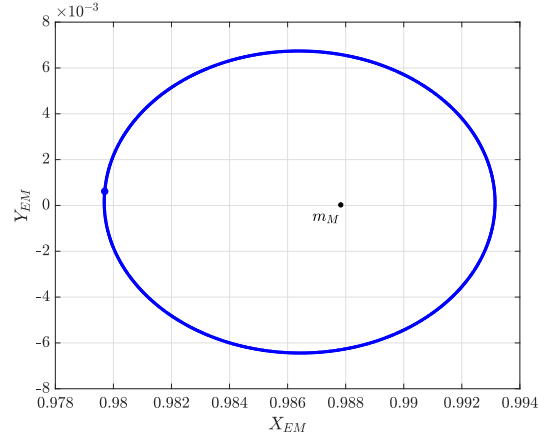
$$(100 + R_{moon}) \cdot 10^3 / DU \leq r_p \leq (500 + R_{moon}) \cdot 10^3 / DU \quad (7.14)$$

$$(500 + R_{moon}) \cdot 10^3 / DU \leq r_a \leq (6000 + R_{moon}) \cdot 10^3 / DU \quad (7.15)$$

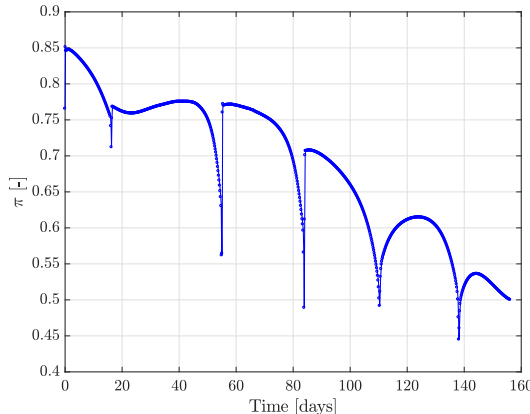
Figure 7.1.4 gathers the results in terms of trajectory, lunar orbit, throttle, thrust direction and mass consumption. The difference between the initial guess and the optimized trajectory can again be attributed to the reasons outlined in Section 7.1.3. As it can be seen in Figure 7.1.4b, which results from integrating the final transfer state onward with no thrust, the final lunar orbit is elliptic, with $h_p = 309$ km and $h_a = 1400$ km. The thrusting is quite continuous and the final mass fraction is $m_f/m_0 = 0.9293$. The impulsive burn required at the initial instant is $\Delta V_0 = 1.1918$ km/s and the transfer time is 156.1 days.



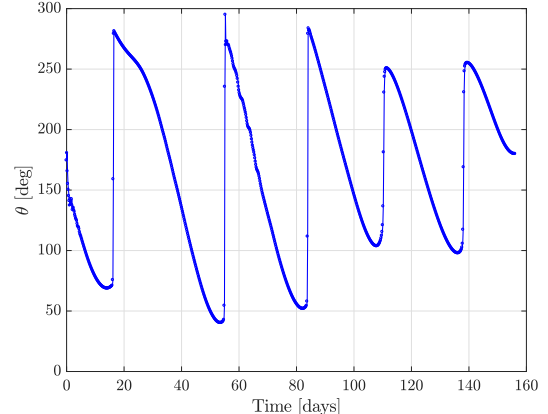
(a) Complete trajectory. (—) Optimized trajectory, (—) Initial guess trajectory.



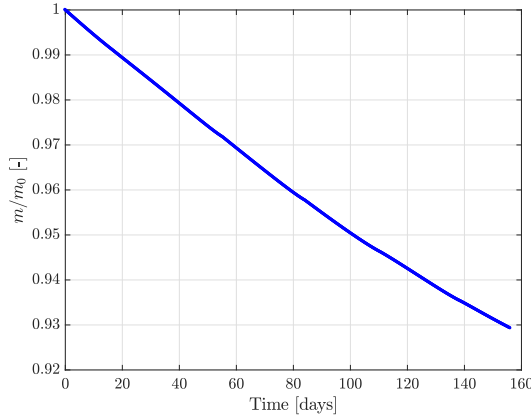
(b) Moon orbit



(c) Throttle evolution



(d) Thrust direction evolution



(e) Mass fraction evolution

Figure 7.1.4: Trajectory D results.

7.2 Trajectory comparison and possible lunar missions

Table 7.2.1 summarizes the details pertaining to the solution trajectories presented in the previous section.

	Initial Guess	ΔV_0	Final lunar orbit	Transfer time	m_f/m_0
A	Two-impulse	1.0508 km/s	Circular, $h_c = 723$ km	63.4 days	0.9895
B	Two-impulse	1.0506 km/s	Elliptical, $h_p = 123$ km, $h_a = 500$ km	63.3 days	0.9805
C	Inv. manifolds	1.2084 km/s	Circular, $h_c = 1835$ km	154.2 days	0.9856
D	Inv. manifolds	1.1918 km/s	Elliptical, $h_p = 309$ km, $h_a = 1400$ km	156.1 days	0.9293

Table 7.2.1: Details of optimized trajectories.

First of all, it is worth mentioning that the trajectory design process presented in this work has led to feasible orbits from the Astrodynamics point of view with both methods for initial guess generation considered. Besides, these trajectories are also consistent when one takes into account the size and propulsion constraints for a nominal Cubesat. Lastly, the fact that the initial guesses are robust enough so that after optimized, the trajectories keep their main initial features is highly advantageous and can ease the preliminary stages of any mission design process.

As it has been explained, trajectories A and B stem from the classical two-impulse transfer initial guess, while solutions C and D have been obtained starting from the initial guess based on the Lagrange invariant manifolds. At the same time, two of them (A and C) lead to final circular lunar orbits while in the other two cases (B and D) the final orbit is elliptic. This variety of final Moon orbits has been intentional and it serves to illustrate the potential of the method and the possibility to tailor it to the mission at hand.

As it can be seen in Table 7.2.1, the two approaches used for initial guess construction have led to eminently different trajectories. Indeed, trajectories obtained from the invariant manifolds initial guess exhibit a longer transfer time, even more than twice the one

offered by the solutions coming from the two-impulse trajectories, and a slightly higher initial impulse. However, we should not discard the invariant manifolds trajectories right away since those are not the only factors that affect trajectory design. Indeed, system-level requirements coming from technology limitations, among others, can sometimes have a great impact on trajectory design and push it towards longer transfer time trajectories. Besides, obtaining initial guesses by exploiting the three-body dynamics provides an unique insight on the trajectories that can be very advantageous to mitigate and correct possible uncertainties or deviations from the preset path.

Practically speaking, the trajectories presented could serve as a basis for the mission analysis phase of many different lunar cubesat future endeavours. Indeed, different kind of moon orbits can be easily reached in an acceptable amount of time and just requiring a reasonable external burn at the initial instant. The variety in the final lunar orbits presented illustrate how those different missions could be designed following a similar approach.

In this way, Trajectories B and D could easily fit lunar exploration missions in which it is necessary to reach lower altitudes to perform the scientific activities, that would be mainly undertaken during periapsis passages. Related examples of past lunar exploration missions are SMART 1, which had an operational orbit of 2200×4600 km (perilune \times apolune distance) [65], or SELENE, which was injected into an $101 \text{ km} \times 11741 \text{ km}$ orbit [66]. As mentioned in Section 2.3, upcoming Cubesat exploration missions include Lunar Flashlight and LunarH-Map, which are expected to operate in elliptical lunar orbits with very low altitude perilunes: 10-30 km and 5-12 km, respectively [19, 20]. In this way, Lunar Flashlight will determine the presence or absence of exposed water ice and map its concentration, while LunaH-Map will map hydrogen in permanently shadowed regions throughout the South Pole, obtaining in both cases information with unprecedent resolution.

Alternatively, circular Moon orbits similar to the ones associated to Trajectories A or C could be appropriate for communication relays. For instance, a 1000-km lunar-orbiting communication satellite relaying signals to and from points up to 200 km above the lunar far-side surface was already discussed in [67]. These kind of missions would indeed be very useful to help establish a lunar orbiting communication and navigation relay infrastructure to support both robotic and long term human lunar missions. Lunar relay satellites can provide lunar vicinity and surface coverage, flexibility and agility in forming connections, and the ability to provide communications and navigation for multiple, concurrent missions [68]. Similar orbits, but probably with higher altitudes, could be used to create a lunar GPS constellation. During the Apollo era, navigation relied on tracking and state updates from the ground. The Orion program, however, is required to navigate autonomously from the ground [69]. In this regard, lunar constellations have been already suggested [24, 70]. For instance, Carpenter *et al* [70] proposes Moon-centered constellations with semi-major axis ranging between 6000 km and 9000 km.

To conclude, it would be interesting to see how this work compares with some other low-thrust transfers presented in the literature, which have been detailed in Chapter 3. However, this is a challenging task since the initial and final orbits might not be the same, and also most studies are oriented towards conventional large spacecraft trajectories. However, a rough comparison shows that the results presented in this project are quite reasonable and coherent with previous works. For instance, Mingotti [57], whose work was also

based on dynamics of the CR3BP libration points -similarly to our initial guess based on the invariant manifold dynamics- reported transfers lasting between 100 and 300 days, with an initial impulse of just over 3 km/s and a required fuel fraction of about 5% for the low-thrust transfer. These results are comparable, in order of magnitude, with the ones obtained for trajectories C and D if one takes into account that in [57], the transfer started at LEO whereas our trajectories start at GEO, hence the difference in the initial impulse required to escape the Earth.

Chapter 8

Project Management

The work presented in this project is eminently technical; however, it could not be completely understood without the socioeconomic context presented in Chapter 2. In the same way, it is indispensable to provide some insight into this project from a managerial point of view. This chapter will be dedicated to it, mainly focusing on the resources needed to be allocated, both in terms of time and cost.

8.1 Time Management

Overall, the project high-level structure became clear very early in the project definition. In this way, the development of this project was divided into three main phases: literature review, initial guess construction and trajectory optimization. Each of them was composed by different tasks described in the Gantt chart in Table 8.1.1. As it can be seen, the project structure did not follow exactly the *waterfall* approach, since the three phases overlapped in time as a consequence of the iterations needed in order to obtain satisfactory results. For instance, initial non-convergences of the optimization algorithm triggered the need to iterate and refine the initial guesses construction.

The complete project spanned around six months, with an approximate total of 500 engineering hours devoted to it. Approximately, the initial problem definition and literature review were performed in the first two and a half months. During this time, the problem was identified and understood in depth, including an exhaustive review of previous work together with the acquisition of the needed background information and concepts. The documentation of this phase was done progressively in parallel with the remaining project phases.

After that, the initial guess construction began. This process took approximately three months and it consisted on fully understanding, implementing and adapting the methods found in the literature to find initial guesses for Earth-Moon transfers. For the initial guess based on the invariant manifolds of the Lagrange points, the greatest effort and time span was devoted to the understanding of the dynamics and the development of a routine that would find the stable and unstable manifolds of two different systems and find a coherent

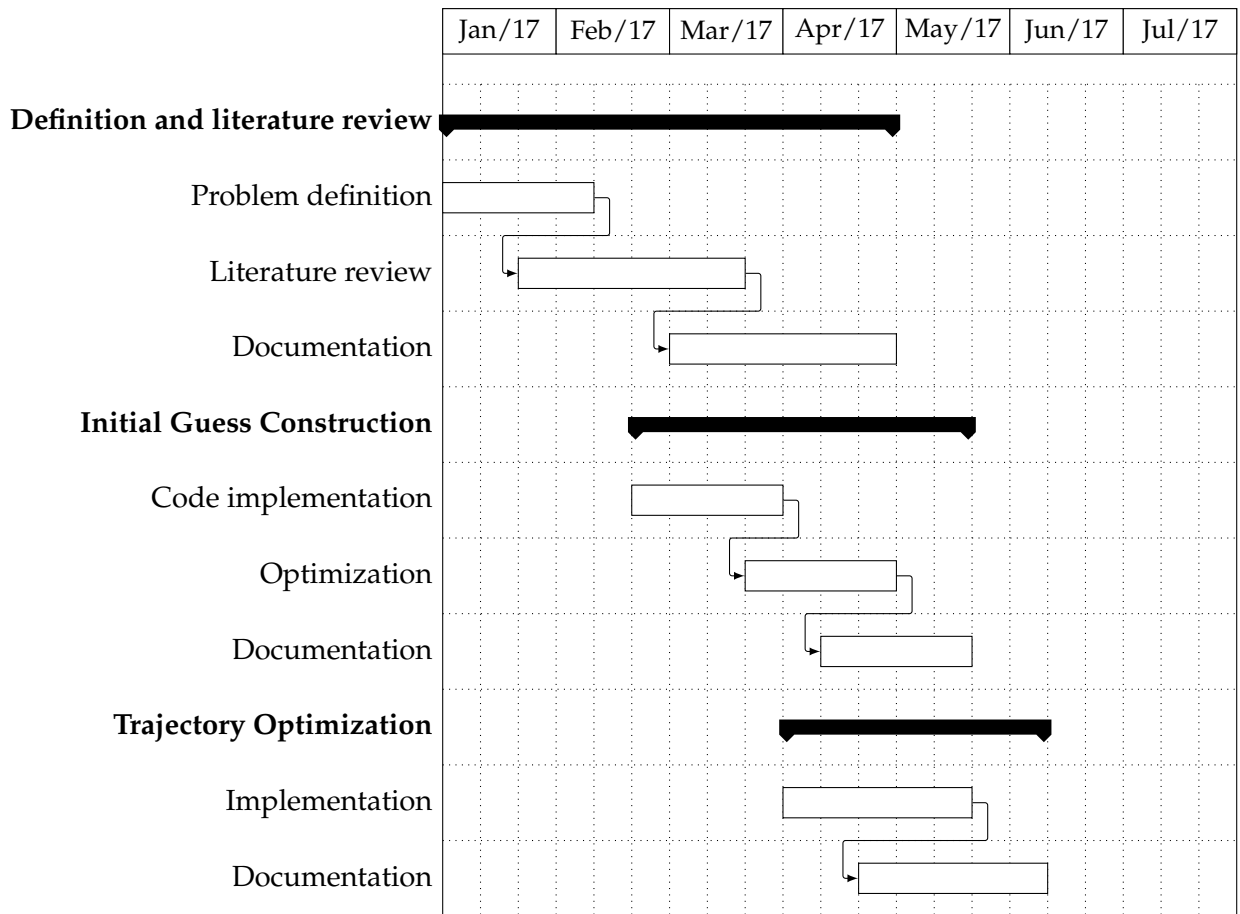


Table 8.1.1: Gantt chart

patching point. For the initial guess based on the four body problem dynamics, the main effort was related to the understanding of how to work with and tune the genetic algorithm in order to find the desired results.

Finally, the last step consisted on defining and implementing the optimization problem starting from the acquired initial guesses. Appropriate tuning of the constraints involved in the optimal control problem definition was needed so that the optimization algorithm could converge to a solution in a reasonable amount of time. This third and final phase of the project lasted approximately two months.

8.2 Cost Management

This section describes all costs associated to the project and proposes an estimate of the budget needed to replicate it.

Most of the incurred costs were direct costs, meaning that they can be specifically attributed to the project. They include the engineering working hours, software licenses, etc.

On the other hand, indirect costs are not that easy to quantify, since they include light, Internet connection,... and will be therefore estimated as a percentage of the direct costs.

Tables 8.2.1 to 8.2.3 include the detailed costs estimation; the final project budget can be found in Table 8.2.4, which amounts to 11570.92 €.

As it can be seen, labor costs reduce to the salary of an Aerospace Engineer, which has been estimated to be 20 €/h; apart from this, equipment and software costs complete the direct costs. Concerning the computer, since it is an asset subject to depreciation, straight line depreciation over a 3 year period has been assumed. Finally, indirect costs have been estimated as a 10% of the total direct costs.

Labor cost			
Item	Price [€/h]	Dedication [h]	Labor cost [€]
Aerospace Engineer	20	500	10000

Table 8.2.1: Labor cost details.

Equipment cost				
Item	Price [€]	Dedication [h]	Depreciation period [h]	Equipment cost [€]
Laptop	1000	500	26280	19.02

Table 8.2.2: Equipment cost details.

Software cost		
Item	Price [€]	Software cost [€]
MATLAB Academic	500	500

Table 8.2.3: Software cost details.

Direct costs	
Labor cost	10000 €
Laptop depreciation	19.02 €
Software cost	500 €
Indirect costs	
Light, Internet connection,...	1051.90 €
Total costs	
11570.92 €	

Table 8.2.4: Total project costs.

Chapter 9

Conclusions and Future Work

The goal of this work has been to provide a trajectory design framework for Earth-Moon Cubesat transfers. This comes from acknowledging the large amount of promising lunar Cubesat initiatives proposed so far and the fact that most of them focus mainly on the system level analysis. However, Cubesat missions also pose many challenges from a trajectory design point of view, mostly due to the sizing and propulsive limitations associated to them.

In this work, a complete procedure to design Earth-Moon Cubesat transfers has been detailed. The results have been very satisfactory since feasible trajectories have been found of reasonable duration and associated fuel mass fraction. Besides, the trajectories presented inject the spacecraft in lunar orbits that are appropriate for Cubesats to be used as lunar communication relays or that carry scientific payloads for exploration missions, among others. Besides, the potential of the proposed method lies mainly on the possibility of tuning it in a simple way in order to adapt it to the requirements of the mission, representing then a powerful tool for trajectory design.

The method proposed can be divided in two main phases: initial guess construction and trajectory optimization. In this project, initial guesses were obtained following well-known approaches in the literature for impulsive Earth-Moon transfers, one of them relying on the dynamics of libration points' invariant manifolds in the PCR3BP; the other one using a more holistic approach in the PBRFBP and genetic optimization. Then, these initial guesses were optimized in the PBRFBP dynamic model in order to obtain complete minimum-fuel trajectories fulfilling all the constraints for a feasible mission from the Astrodynamics point of view.

However, it is worth mentioning that although the results presented here are perfectly valid for a mission feasibility analysis, later stages of the mission design will require more detailed trajectory analysis. Future work emanates naturally from this mission work flow, and should be aimed at obtaining more realistic optimized trajectories for which some of the assumptions used in this work might not hold. For instance, the dynamic model in which the NLP optimization is performed might need to be modified to include the contribution of perturbations, such as Earth oblateness effect or solar radiation pressure. Following the same line of thought, an optimization in the the full 3D four body dynamic model could

provide some more insight on the Earth-Moon transfer problem. Moreover, for any given mission, system level requirements can heavily impact trajectory design, meaning that the optimal trajectory from a purely Astrodynamical standpoint might not be the preferred one at later stages of the mission design.

To conclude, this project does not pretend to be an exhaustive collection of possible Cubesat Earth-Moon transfers but rather a proof of concept that this kind of trajectories are feasible, enabling then this newly envisioned low-cost, fast development lunar exploration missions.

Bibliography

- [1] E. Mabrouk, “What are SmallSats and CubeSats?.” <https://www.nasa.gov/content/what-are-smallsats-and-cubesats>, 2015.
- [2] “NASA Selects CubeSat, SmallSat Mission Concept Studies.” <https://www.nasa.gov/feature/nasa-selects-cubesat-smallsat-mission-concept-studies>, 2017.
- [3] K. Woellert, P. Ehrenfreund, A. J. Ricco, and H. Hertzfeld, “Cubesats: Cost-effective science and technology platforms for emerging and developing nations,” *Advances in Space Research*, vol. 47, no. 4, pp. 663–684, 2011.
- [4] Cal Poly SLO, “Cubesat Design Specification (CDS),” *The CubeSat Program*, no. 13, 2014.
- [5] A. Toorian, K. Diaz, and S. Lee, “The CubeSat approach to space access,” in *IEEE Aerospace Conference Proceedings*, 2008.
- [6] K. Lemmer, “Propulsion for CubeSats,” *Acta Astronautica*, vol. 134, no. January, pp. 231–243, 2017.
- [7] W. P. Wright and P. Ferrer, “Electric micropropulsion systems,” *Progress in Aerospace Sciences*, vol. 74, pp. 48–61, 2015.
- [8] D. R. Lev, G. D. Emsellem, and A. K. Hallock, “The Rise of the Electric Age for Satellite Propulsion,” *New Space*, vol. 5, no. 1, pp. 4–14, 2017.
- [9] C. Collingwood, *Investigation of a Miniature Differential Ion Thruster*. PhD thesis, University of Southampton, 2011.
- [10] S. Spangelo, B. Longmier, and D. Dalle, “Integrated Vehicle and Trajectory Design of Small Spacecraft with Electric Propulsion for Earth and Interplanetary Missions,” in *Small Satellite Conference*, (Logan, Utah), 2015.
- [11] J. Mueller, J. Ziemer, R. Hofer, R. Wirz, and T. O'Donnell, “A survey of micro-thrust propulsion options for microspacecraft and formation flying missions,” in *5th Annual CubeSat Developers Workshop*, (San Luis Obispo, CA), 2008.
- [12] A. V. Loyal and T. A. Maksymenko, “Performance Investigation of SPT-20M Low Power Hall Effect Thruster,” in *30th International Electric Propulsion Conference*, (Florence, Italy), 2007.

- [13] BUSEK Space Propulsion and Systems, "Pulsed Plasma Thrusters." http://www.busek.com/technologies_ppt.htm.
- [14] Earth Observation Portal, "FalconSat-3." <https://directory.eoportal.org/web/eoportal/satellite-missions/f/falconsat-3>.
- [15] BUSEK Space Propulsion and Systems, "BET-100 Busek Electrospray Thruster." http://www.busek.com/index_htm_files/70008516F.PDF, 2016.
- [16] I. A. Crawford and K. H. Joy, "Lunar exploration: opening a window into the history and evolution of the inner Solar System.," *Philosophical transactions of the Royal Society. Series A, Mathematical, physical, and engineering sciences*, vol. 372, p. 20130315, 2014.
- [17] Lunar Exploration Analysis Group, "Strategic Knowledge Gap Special Action Team Review," in *LEAG Gap Review*, pp. 1–70, 2016.
- [18] R. W. Conversano and R. E. Wirz, "CubeSat Lunar Mission Using a Miniature Ion Thruster," in *47th AIAA/ASME/SAE/ASEE Joint Propulsion Conference & Exhibit*, (San Diego, CA), American Institute of Aeronautics and Astronautics, 2011.
- [19] J. Harbaugh, "LunaH-Map: University-Built CubeSat to Map Water-Ice on the Moon." <https://www.nasa.gov/feature/lunah-map-university-built-cubesat-to-map-water-ice-on-the-moon>, 2016.
- [20] P. O. Hayne, B. A. Cohen, B. T. Greenhagen, D. A. Paige, J. M. Camacho, R. G. Sellar, and J. Reiter, "Lunar Flashlight: Illuminating the Moon's South Pole," in *47th Lunar and Planetary Science Conference*, (The Woodlands, TX), 2016.
- [21] T. Fleischman, "Cornell's quest: Make the first CubeSat to orbit the moon." <http://www.news.cornell.edu/stories/2016/09/cornells-quest-make-first-cubesat-orbit-moon>, 2016.
- [22] R. T. Rajan, S. Engelen, M. Bentum, and C. Verhoeven, "Orbiting low frequency array for radio astronomy," in *IEEE Aerospace Conference Proceedings*, 2011.
- [23] J. Rotteveel, B. Chamot, M. Bentum, M. K. Wolt, and A. J. Boonstra, "A road map for low frequency radio astronomy in lunar orbit using CubeSats," in *6th Interplanetary CubeSat Workshop*, (Cambridge, UK), may 2017.
- [24] P. A. Stadter, D. J. Duven, B. L. Kantsiper, P. J. Sharer, E. J. Finnegan, and G. L. Weaver, "A Weak-signal GPS Architecture for Lunar Navigation and Communication Systems," in *IEEE Aerospace Conference Proceedings*, 2008.
- [25] L. Zhang and P. Wang, "Communication Relay and Navigation Micro Satellite for Lunar South Pole Landing Exploration Mission," in *6th Interplanetary CubeSat Workshop*, (Cambridge, UK), may 2017.
- [26] A. Batista, E. Gomez, H. Qiao, and K. E. Schubert, "Constellation Design of a Lunar Global Positioning System Using CubeSats and Chip-Scale Atomic Clocks Constellation Design of a Lunar Global Positioning System Using CubeSats and Chip-Scale Atomic Clocks," in *Proceedings of the International Conference on Embedded Systems and Applications (ESA)*, no. January, 2012.

- [27] K. P. Zondervan, *Optimal Low Thrust, Three Burn Orbit Transfers With Large Plane Changes*. PhD thesis, California Institute of Technology, 1983.
- [28] J. E. Marsden, M. W. Lo, W. S. Koon, and S. D. Ross, *Dynamical Systems, the Three-Body Problem and Space Mission Design*. 2006.
- [29] E. a. Belbruno and J. K. Miller, "Sun-perturbed Earth-to-moon transfers with ballistic capture," *Journal of Guidance, Control, and Dynamics*, vol. 16, no. 4, pp. 770–775, 1993.
- [30] F. Topputto, "On optimal two-impulse Earth-Moon transfers in a four-body model," *Celestial Mechanics and Dynamical Astronomy*, vol. 117, no. 3, pp. 279–313, 2013.
- [31] E. Belbruno, *The Dynamical Mechanism of Ballistic Lunar Capture Transfer in the Four-body Problem from the Perspective of in Variant Manifolds and Hill's Regions*. 1994.
- [32] W. S. Koon, M. W. Lo, J. E. Marsden, and S. D. Ross, "Low Energy Transfer to the Moon," *Celestial Mechanics and Dynamical Astronomy*, vol. 81, pp. 63–73, 2001.
- [33] C. C. Conley, "Low Energy Transit Orbits in the Restricted Three-Body Problems," *SIAM Journal on Applied Mathematics*, vol. 16, no. 4, pp. 732–746, 1968.
- [34] D. C. Redding and J. V. Breakwell, "Optimal Low-Thrust Transfers To Synchronous Orbit," *Journal of Guidance, Control, and Dynamics*, vol. 7, no. 2, pp. 148–155, 1984.
- [35] O. M. Golan and J. V. Breakwell, "Minimum Fuel Lunar Trajectories for a Low-Thrust Power-Limited Spacecraft," *Dynamics and Control*, vol. 4, pp. 383–394, 1994.
- [36] B. L. Pierson and C. A. Kluever, "Three-Stage Approach to Optimal Low-Thrust Earth-Moon Trajectories," *Journal of Guidance, Control, and Dynamics*, vol. 17, no. 6, pp. 1275–1282, 1994.
- [37] A. L. Herman and B. A. Conway, "Optimal, Low-Thrust, Earth-Moon Orbit Transfer," *Journal of Guidance, Control, and Dynamics*, vol. 21, no. 1, 1998.
- [38] E. A. Belbruno, "Lunar Capture Orbits, a Method of Constructing Earth Moon Trajectories and the Lunar Gas Mission," in *19th AIAA/DGLR/JSASS International Electric Propulsion Conference*, (Colorado Springs, Colorado), 1987.
- [39] G. Mingotti, F. Topputto, and F. Bernelli-Zazzera, "Low-energy, low-thrust transfers to the Moon," *Celestial Mechanics and Dynamical Astronomy*, vol. 105, no. 1, pp. 61–74, 2009.
- [40] A. Ohndorf, B. Dachwald, and E. Gill, "Optimization of Low-Thrust Earth-Moon transfers using Evolutionary Neurocontrol," in *2009 IEEE Congress on Evolutionary Computation, CEC 2009*, pp. 358–364, 2009.
- [41] J. T. Betts and S. O. Erb, "Optimal Low Thrust Trajectories to the Moon," *SIAM Journal on Applied Dynamical Systems*, vol. 2, no. 2, pp. 144–170, 2003.
- [42] J. Schoenmaekers, D. Horas, and J. A. Pulido, "SMART-1 with Solar Electric Propulsion to the Moon," in *16th International Symposium on Space Flight Dynamics*, (Pasadena, CA), 2001.

- [43] N. Sullo, P. A. De Sousa-Silva, M. O. Terra, and M. Ceriotti, "Optimization of Low-Thrust and Hybrid Earth-Moon Transfers," in *67th International Astronautical Congress*, (Guadalajara, Mexico), 2016.
- [44] B. Dachwald, "Evolutionary Neurocontrol: A Smart Method for Global Optimization of Low-Thrust Trajectories," in *AIAA/AAS Astrodynamics Specialist Conference and Exhibit*, (Providence, Rhode Island), 2004.
- [45] S. Campagnola, N. Ozaki, Q. Verspieren, K. Oguri, K. Kakihara, K. Yanagida, R. Funase, C. H. Yam, L. Ferella, T. Yamaguchi, Y. Kawakatsu, and D. Garcia Yarnoz, "Mission Analysis for JAXA's Earth-Moon Libration-Orbit Cubesat," in *67th International Astronautical Congress*, 2016.
- [46] W. D. Lakin and C. Brandon, "Landing a CubeSat payload on the moon: The Vermont Space Grant Lunar Lander Project," *Design Principles and Practices*, vol. 5, no. 3, 2011.
- [47] D. C. Folta, N. Bosanac, A. Cox, and K. C. Howell, "The Lunar IceCube Mission Design: Construction of Feasible Transfer Trajectories with a Constrained Departure," in *26th AAS/AIAA Space Flight Mechanics Meeting*, (Napa, CA), 2016.
- [48] H. Schaub and J. L. Junkins, *Analytical Mechanics of Aerospace Systems*. 2002.
- [49] K. Yagasaki, "Sun-perturbed Earth-to-Moon transfers with low energy and moderate flight time," *Celestial Mechanics and Dynamical Astronomy*, vol. 90, no. 3, pp. 197–212, 2004.
- [50] J. D. Hadjidemetriou, "Periodic Orbits in Gravitational Systems." <http://users.auth.gr/hadjidem/cortina.pdf>.
- [51] J. Marsden, "Invariant Manifolds." <http://www.cds.caltech.edu/~marsden/wiki/uploads/cds140a-09/lecturenotes/InvariantManifolds.pdf>.
- [52] K. E. Davis, R. L. Anderson, D. J. Scheeres, and G. H. Born, "The use of invariant manifolds for transfers between unstable periodic orbits of different energies," *Celestial Mechanics and Dynamical Astronomy*, vol. 107, no. 4, pp. 471–485, 2010.
- [53] S. C. Spangelo, D. Dalle, and B. W. Longmier, "Small Spacecraft System-level Design and Optimization for Interplanetary Trajectories," in *AIAA/AAS Astrodynamics Specialist Conference*, (San Diego, CA), 2014.
- [54] K. Jayavani and G. Nawaz, "Study of Genetic Algorithm, an Evolutionary Approach," *International Journal on Recent and Innovation Trends in Computing and Communication*, vol. 2, no. 8, pp. 2331–2334, 2014.
- [55] A. Seshadri, "A Fast Elitist Multiobjective Genetic Algorithm: NSGA-II," *Matlab Central File Exchange*, 2007.
- [56] J. T. Betts, "A Survey of Numerical Methods for Trajectory Optimization," *Journal of Guidance, Control, and Dynamics*, vol. 21, no. 2, pp. 193–207, 1998.
- [57] G. Mingotti, F. Topputo, and F. Bernelli-Zazzera, "Numerical Methods to Design Low-Energy, Low-Thrust Sun-Perturbed Transfers to the Moon," in *49th Israel Annual Conference on Aerospace Sciences*, (Tel Aviv–Haifa, Israel), pp. 1–14, 2009.

- [58] A. V. Rao, "A survey of numerical methods for optimal control," *Advances in the Astronautical Sciences*, vol. 135, no. 1, pp. 497–528, 2009.
- [59] G. A. Bliss, "Lectures on the Calculus of Variations," 1946.
- [60] R. Hannemann-Tamás and W. Marquardt, "How to verify optimal controls computed by direct shooting methods? - A tutorial," *Journal of Process Control*, vol. 22, no. 2, pp. 494–507, 2012.
- [61] A. V. Rao, G. T. Huntington, D. Benson, C. L. Darby, C. Francolin, M. Patterson, and I. Sanders, "Users Manual for GPOPS Version 2.3: A MATLAB Software for Solving Multi-Phase Optimal Control Problems Using the Gauss Pseudospectral Method," 2009.
- [62] F. Topputo and C. Zhang, "Survey of direct transcription for low-thrust space trajectory optimization with applications," *Abstract and Applied Analysis*, 2014.
- [63] Y. Kawajir, C. D. Laird, A. Waechter, and F. Margot, "Introduction to IPOPT: A tutorial for downloading, installing, and using IPOPT," 2013.
- [64] A. Wächter, *An Interior Point Algorithm for Large-Scale Nonlinear Optimization with Applications in Process Engineering*. PhD thesis, Carnegie Mellon University, 2002.
- [65] B. H. Foing, O. Camino, J. Schoenmakers, J. de Bruin, D. Gestal, M. Alonso, R. Blake, S. Ricken, P. Pardo, D. Koschny, D. Frew, M. Almeida, M. Sarkarati, J. Volp, G. H. Schwehm, J. L. Josset, S. Beauvivre, Z. Sodnik, M. Grande, U. Keller, A. Nathues, P. Ehrenfreund, and G. D. Racca, "SMART-1 Mission Overview from Launch, Lunar Orbit to Impact," in *38th Lunar and Planetary Science Conference*, (League City, Texas), 2007.
- [66] Japan Aerospace Exploration Agency (JAXA), "KAGUYA (SELENE) Result of the Lunar Orbit Injection Maneuver." http://global.jaxa.jp/press/2007/10/20071005_kaguya_e.html, 2007.
- [67] P. E. Schmid, "Lunar Far-Side Communication Satellites," *NASA TN D-4509*, 1968.
- [68] K. B. Bhasin, A. W. Hackenberg, R. A. Slywczak, P. Bose, M. Bergamo, and J. L. Hayden, "Lunar Relay Satellite Network for Space Exploration: Architecture, Technologies and Challenges," in *24th AIAA International Communications Satellite Systems Conference, ICSSC*, (San Diego, CA), 2006.
- [69] R. Zanetti, B. Crouse, and C. D'Souza, "Autonomous optical lunar navigation," in *AAS Spaceflight Mechanic Conference*, (Georgia, United States), 2009.
- [70] J. R. Carpenter, D. C. Folta, M. C. Moreau, and D. A. Quinn, "Libration Point Navigation Concepts Supporting the Vision for Space Exploration," in *AIAA/AAS Astrodynamical Conference*, (Providence, RI), 2004.